Institute of
Applied Mechanics
Institut für Baumechanik

Graz University of Technology

Preprint Series

Institute of Applied Mechanics

Graz University of Technology

Preprint No 2/2010

Infinite elements in a poroelastodynamic FEM

M. Nenning, M. Schanz
Institute of Applied Mechanics, Graz University of Technology

published in *International Journal for Numerical and Analytical Methods in Geomechanics*, **35**(16), 1774–1800,2011

Latest revision: October 15, 2011

Abstract

An infinite element is presented to treat wave propagation problems in unbounded saturated porous media. The porous media is modeled by Biot's theory. Conventional finite elements are used to model the near field, whereas infinite elements are used to represent the behavior of the far field. They are constructed in such a way that the Sommerfeld radiation condition is fulfilled, i.e., the waves decay with distance and are not reflected at infinity. To provide the wave information the infinite elements are formulated in Laplace domain. The time domain solution is obtained by using the convolution quadrature method as inverse Laplace transformation. The temporal behavior of the near field is calculated using standard time integration schemes, e.g., the Newmark-method. Finally, the near- and far field are combined using a substructure technique for any time step. The accuracy as well the necessity of the proposed infinite elements, when unbounded domains are considered, will be demonstrated by different examples.

1 Introduction

The numerical treatment of unbounded domains is of considerable interest in many engineering applications, e.g., soil structure analysis, earthquake- or geotechnical engineering. The use of so called infinite elements together with the well known Finite Element Method (FEM) is a possible choice for the investigation of such unbounded domains. An infinite element is simply an element which attempts to represent the behavior of the solution in the unbounded domain. Infinite elements are easily coupled to finite elements and retain the banded structure of finite element matrices. Nevertheless, various other numerical methods for unbounded domains exists. An overview of such methods is for example given in the book of Givoli [27].

One common choice for the numerical treatment of unbounded domains is the Boundary Element Method (BEM). A significant point of the BEM is the use of so called fundamental solutions, which are analytical solutions of the governing differential equations due to a point source within an unbounded domain. The fact that the fundamental solution is exact brings in the advantage of improved accuracy. Nevertheless, the BEM is restricted to linear differential equations since the fundamental solutions for non-linear problems are not attainable in general. A common approach to deal with non-linear problems is the coupling of BEM with FEM [51]. Moreover, singularities are present using the boundary element method, which need special attention for the numerical integration. The application of the BEM for the poroelastic case is elaborated in detail by Schanz [44]. Besides the BEM there also exist other numerical methods which try to approximate the unbounded domain.

One common approach is the use of so called artificial or absorbing boundary conditions (ABC). This method introduces an artificial boundary to deceive the solution that it actually extends to infinity. To find proper choices of boundary conditions for various wave problems is not trivial since the artificial boundary condition has to represent the unbounded domain in an appropriate manner. In the context of wave propagation problems, an artificial boundary condition is also called a *Non-Reflecting Boundary Condition (NRBC)*. Various non-reflecting boundary conditions have been proposed in the literature, e.g. [26]. A classical approximate absorbing boundary is developed by Lysmer and Kuhlemeyer [35] and consists of a viscous dashpot model. Although this model is local and cheaply computed, it requires large bounded domains for satisfactory accuracy. Even more, this model is only capable to absorb incident waves on a small range of incidence angles.

The unbounded domain can also be represented by using an absorbing boundary layer. Whenever a traveling wave enters the absorbing layer it is attenuated by the absorbing layer and, therefore, it's amplitude decreases. Nevertheless, the thickness of the boundary layer as well as the absorbing properties remain to be chosen in such a way that waves are absorbed sufficiently. This characteristic yields the denotation *Perfectly Matched Layer*, or *PML*, for the absorbing layer. The PML was first initiated by Berenger [13] for the application to electromagnetism (Maxwell's equations). Various interpretations of the PML are offered by different authors, e.g. [19, 61, 43]. The most popular interpretation of the PML is the co-ordinate stretching explanation, provided by Chew et al. [19]. Various application of the PML exist, e.g. the transient and time-harmonic case for elastodynamics is discussed for example by Basu and Chopra [10, 9, 8]. Poroelastic material using perfectly matched layers is treated by Zeng et al. [57].

Another approximation method to deal with unbounded domains is the use of infinite ele-

ments, which will be discussed in the following in more detail. First publications on infinite elements were the thesis of Ungless [50] and the paper of Zienkiewicz and Bettess [62]. There exist mainly two different types of infinite elements. First, the use of a *decay function* together with a shape function which causes the field quantity to approach the sought value at infinity, while the finite size of the infinite element is retained. Second, conventional shape function are used to describe the variation of the field quantity, while the geometry is mapped from a finite to an infinite domain. Using the latter, brings in the advantage that the application of standard integration formulas is possible, e.g., standard Gauß integration [65]. Mapped infinite elements perform well for the static case in elastic media [65]. Such mapped infinite elements were also applied successfully to quasi-static materially nonlinear problems [37]. The application of infinite elements to wave propagation problems makes it necessary to include outwardly propagating wave-like factors in their formulation. This concept was originally proposed by Zienkiewicz and Bettess [14]. For acoustic media a wide variety of formulations exists and are well developed. A comprehensive overview for the acoustic case is given by Astley [4]. Whereas in the acoustic case only one traveling wave is present, in a homogeneous elastic halfspace there are actually three distinct waves, in particular shear-, compressional-, and Rayleigh waves. If a layered halfspace is considered also Love waves may occur [28]. These waves travel with different wave speeds. However, the simplest approach is to include only the characteristic of one wave within the infinite element formulation. Depending on the spatial location of the infinite element, the dominant wave is consequently incorporated into the infinite element formulation. Moreover, an exponential decay of the field quantity is often assumed, instead of the correct asymptotic decay in three dimensions of $1/r$ (r is the distance measure to the applied load) [60, 55]. Infinite elements, capable of simulating all three wave types in the time harmonic case are developed by Zhao and Valliappan [58] and Yun et al. [56], but they also assume an exponential decay of the solution. Medina et al. [38] proposed an interesting infinite element, considering all three wave types. They performed very well but the evaluation of the shape functions turned out to be extremely tedious.

An infinite element formulation for wave propagation problems in one-dimensional poroelastic material has been accomplished by Khalili [31]. Later he extended his work to the two-dimensional case [32]. His work covers time harmonic problems and the infinite element formulation only considers the occurrence of the two compressional waves.

Of course, the application of infinite elements is widespread and applied to many different fields of engineering. Here are some examples in compressed form such as consolidation [48], mass transport [59], electromagnetic [25], heat transfer [49], ground freezing [3], fluid-structure interaction [66, 14], and soil-structure interaction [20, 38, 39, 41, 21, 55, 56].

In the following, an infinite element will be presented, capable of handling all waves that are present in an unbounded saturated porous media. The saturated porous media is modeled in terms of Biot's theory [16, 15]. The developed infinite element is of the mapped type to ensure the correct asymptotic decay for the three-dimensional case. Although, the approach of the infinite element is rather simple as will be seen in the ongoing, the numerical results are sufficiently accurate.

Throughout this work, the indical notation is used. The summation convention is applied over repeated indices and Latin indices receive the values 1, 2, 3 in three-dimensions ($3D$). Commas $()_{,i}$ denote spatial derivatives and dots $\dot{()}$ denote the time derivative. The symbol δ_{ij} denotes the

Kronecker-Delta.

2 Biot's theory of linear poroelasticity

Consider a fully saturated porous medium in terms of Biot's theory [16]. The total stress within the porous material reads as

$$\sigma_{ij}^{\text{tot}} = C_{ijk\ell} u_{k,\ell} - \alpha \delta_{ij} p \ , \tag{1}$$

where u_k and p denote the solid displacement and the pore pressure, respectively. The fourth order material tensor $C_{ijk\ell}$ of the solid skeleton is for the case of a homogeneous isotropic elastic material given as

$$C_{ijk\ell} = \left(K - \frac{2}{3} G \right) \delta_{ij} \delta_{k\ell} + G \left(\delta_{ik} \delta_{j\ell} + \delta_{i\ell} \delta_{jk} \right) \ ,$$

with the compression- and shear modulus of the solid skeleton K and G. Note that in the constitutive law (1) small strains are assumed. Furthermore, Biot's effective stress coefficient $\alpha = 1 - {}^{K}/_{K^s}$ is introduced, with K^s denoting the compression modulus of the solid grains. The conservation of mass of the fluid phase is given by the continuity equation

$$q_{i,i} + \alpha \dot{u}_{i,i} + \frac{\phi^2}{R} \dot{p} = 0 \ , \tag{2}$$

where q_i denotes the flux, ϕ the porosity of the porous media and R the compressibility parameter, defined by

$$R = \frac{\phi^2 K^f (K^s)^2}{K^f (K^s - K) + \phi K^s (K^s - K^f)} \ ,$$

with K^f denoting the compression modulus of the fluid phase.

2.1 Governing equations

The governing equations for low frequency applications are [67]

$$\sigma_{ij,j}^{\text{tot}} = \rho \ddot{u}_i \tag{3a}$$

$$q_i = -\kappa (p_{,i} + \rho_f \ddot{u}_i) \ , \tag{3b}$$

when body forces are neglected. In equations (3), κ denotes the permeability, ρ the density of the bulk material, and ρ_f the density of the interstitial fluid. The above approximation is valid for most problems of earthquake analysis and frequencies lower than this [67, 64]. Zienkiewicz et al. [64] discussed based on an one-dimensional example the limitations of the above introduced governing equations (3), where some fluid inertia terms are neglected. The authors conclude that the simplified model (3) does not significantly differ from the complete Biot theory [16], when applied to low frequency problems, as it is mostly the case in soil- or geomechanical problems.

2.2 Plane body waves in poroelastic media

In order to define the shape functions of an infinite element, the different types of body waves which occur in the underlying porous media as well their wave speeds need to be known. Thus, in this section plane body waves are investigated. Consider the following ansatz for a plane wave in Laplace domain

$$\hat{u}_i = A_i \mathrm{e}^{-\frac{s}{c} n_k x_k} \qquad\qquad \hat{p} = B \mathrm{e}^{-\frac{s}{c} n_k x_k} \tag{4}$$

for the solid displacement and the pore pressure, respectively. The symbol $\hat{()}$ denotes the Laplace transformed variable and s is the Laplace parameter. Here, $A_i n_i$ and B give the amplitude of the wave. Since the fluid can only transmit compressional waves the particle displacement is in direction of the traveling wave and may be defined through a scalar value $B = B_k n_k$. The wave normal unit vector is given by n_k and x_k denotes the position vector. Such a solution (4) describes the propagation of plane waves with the wave velocity c in a porous infinite medium, whose wave fronts are perpendicular to the normal vector n_k. Inserting the ansatz (4) into the Laplace transformed equations (3) yields under the assumption of vanishing initial conditions

$$G A_i n_j n_j \frac{s}{c^2} + (K + \frac{1}{3} G) A_j n_j n_i \frac{s}{c^2} - \alpha B n_i \frac{1}{c} - s\rho A_i = 0 \tag{5a}$$

$$-\kappa \frac{s}{c^2} B n_i n_i - \frac{s^2}{c} \kappa \rho_f A_i n_i + \frac{s}{c} \alpha A_i n_i + \frac{\phi^2}{R} B = 0 \,. \tag{5b}$$

Consider now the case that the particle motion is parallel to the propagation of the wave, i.e, $A_i n_i$ is the amplitude of the propagating wave. From equation (5b) the amplitude B can be expressed as

$$B = \frac{Rsc\left[\alpha - \kappa \rho_f s\right]}{Rs\kappa - c^2 \phi^2} A_i n_i \,. \tag{6}$$

Inserting (6) into (5a) and taking into account that $n_i n_i = 1$ and $A_i = A_j n_j n_i$ will lead to an equation for the wave velocity c

$$\left[\frac{1}{c^2}\left(K + \frac{4}{3} G\right) - \frac{R\alpha\left[\alpha - \kappa\rho_f s\right]}{Rs\kappa - c^2\phi^2} - \rho\right] A_i = 0 \,. \tag{7}$$

Equation (7) can only be satisfied if the term in the square brackets vanishes. Hence, from (7) two compressional waves are obtained with the wave speeds

$$\begin{aligned} c_{1,2}^2 = & \frac{R\left(\alpha^2 + s\kappa\rho - s\alpha\kappa\rho_f\right) + (K + \frac{4}{3}G)\phi^2}{2\phi^2\rho} \\ & \pm \frac{\sqrt{\left[R\left(\alpha^2 + s\kappa\rho - s\alpha\kappa\rho_f\right) + (K + \frac{4}{3}G)\phi^2\right]^2 - 4(K + \frac{4}{3}G)Rs\kappa\rho\phi^2}}{2\phi^2\rho} \,. \end{aligned} \tag{8}$$

Considering the case that the particle motion is perpendicular to the direction of wave propagation, i.e., $A_i n_i = 0$, equation (5a) simplifies to

$$\frac{s^2}{c^2}\left[G - c^2\rho\right] A_i = 0 \tag{9}$$

and implies also that the amplitude B in equation (6) vanishes. From equation (9) follows the shear wave speed

$$c_S^2 = \frac{G}{\rho} \,. \tag{10}$$

Since the compressional waves speeds c_1 and c_2 are frequency dependent they are also called *dispersive* waves. In other words, each frequency component propagates with its own velocity. The shear wave velocity c_S on the contrary is non-dispersive.

2.2.1 Rayleigh surface wave

Lord Rayleigh [42] first investigated a surface wave, with the property that their effect decreases rapidly with depth and their velocity of propagation is smaller than that of the body waves. For the case of an elastic material the *Rayleigh wave* speed c_R can be approximated by

$$\frac{c_R}{c_S} = \frac{0.87 + 1.12\nu}{1+\nu} \,, \tag{11}$$

where ν denotes the Poisson's ratio. This approximation can also be applied to porous material as long as low frequency problems are considered, as investigated by Yang [54]. This is the case for many soil- and geomechanical applications.

3 Finite Element Formulation

The Finite Element formulation for the governing equations (3) with (2) can be obtained by a standard variational approach as it is well described in many textbooks, e.g. [68, 29], and will be shown here only perfunctory. The semi-discretized form of the variational approach is obtained by the spatial approximation of the unknown variables as

$$u_i \approx \varphi^m u_i^m \,, \qquad p \approx \vartheta^m p^m \,,$$

where φ^m and ϑ^m denote appropriate shape functions for the solid displacement u_i and the pore pressure p. Discretized variables can be distinguished from continuous one by the superscript, e.g. $()^m$. Moreover, the shape functions φ^m and ϑ^m need not to be chosen equal but if not otherwise stated, they will be chosen to be of of the same order [47, 63]. Note that both shape functions have to possess at least C_0 continuity [68], since the solid displacement and the pore pressure will occur as first derivatives in the variational formulation. For the undrained limit it is known that instabilities can occur [34]. To avoid them the Babuška-Brezzi condition should be satisfied [6, 7, 17]. For a more profound illustration of the proper choice of shape functions the reader is referred to works, e.g. [68, 29, 36]. Moreover, the test function of the variational approach are discretized spatially in the following form

$$\bar{u}_i \approx \varphi^n \bar{u}_i^n \,, \qquad \bar{p} \approx \vartheta^n \bar{p}^n \,,$$

where the symbol $\bar{()}$ denotes the corresponding test function. Inserting the spatial discretizations in a variational approach of the governing equations (3) with the flux of (2), yields a set of algebraic equations of the form

$$\begin{aligned} K_{ik}^{nm} u_k^m - G1_i^{nm} p + M1_{ik}^{nm} \ddot{u}_k^m &= (f_i^n)^u \\ G2^{nm} p^m + M2_k^{nm} \ddot{u}_k^m + C_k^{nm} \dot{u}_k^m + P^{nm} \dot{p}^m &= (f^n)^p \end{aligned} \tag{12}$$

for the bulk material and the fluid phase, respectively. The single components of the algebraic equations on the left hand side are defined as

$$\begin{aligned} K_{ik}^{nm} &= \int_{\widehat{\tau}_e} \varphi_{,j}^n C_{ijk\ell} \varphi_{,\ell}^m \, \mathcal{J}_e \, \mathrm{d}\boldsymbol{\xi} \\ G1_i^{nm} &= \alpha \int_{\widehat{\tau}_e} \varphi_{,i}^n \vartheta^m \, \mathcal{J}_e \, \mathrm{d}\boldsymbol{\xi} \\ M1_{ik}^{nm} &= \rho \delta_{ik} \int_{\widehat{\tau}_e} \varphi^n \varphi^m \, \mathcal{J}_e \, \mathrm{d}\boldsymbol{\xi} \\ G2^{nm} &= \kappa \int_{\widehat{\tau}_e} \vartheta_{,i}^n \vartheta_{,i}^m \, \mathcal{J}_e \, \mathrm{d}\boldsymbol{\xi} \\ M2_k^{nm} &= \kappa \rho_f \int_{\widehat{\tau}_e} \vartheta_{,k}^n \varphi^m \, \mathcal{J}_e \, \mathrm{d}\boldsymbol{\xi} \\ C_k^{nm} &= \alpha \int_{\widehat{\tau}_e} \vartheta^n \varphi_{,k}^m \, \mathcal{J}_e \, \mathrm{d}\boldsymbol{\xi} \\ P^{nm} &= \frac{\phi^2}{R} \int_{\widehat{\tau}_e} \vartheta^n \vartheta^m \, \mathcal{J}_e \, \mathrm{d}\boldsymbol{\xi} \,, \end{aligned} \tag{13}$$

where $\widehat{\tau}_e$ is the corresponding reference element to the element τ_e in the physical space. The determinant of the *Jacobian matrix* is denoted by $\mathcal{J}_e$ and occurs due to the mapping of the finite element from the physical space τ_e to the reference element $\widehat{\tau}_e$ defined on the interval with local coordinates $\xi_i \in [-1,1]$. The components of the right hand side are

$$\begin{aligned} (f_i^n)^u &= \int_{\widehat{\Upsilon}_b} \varphi_\Gamma^n t_i^{\mathrm{tot}} \, \mathcal{J}_b \, \mathrm{d}\boldsymbol{\xi} \\ (f^n)^p &= -\int_{\widehat{\Upsilon}_b} \vartheta_\Gamma^n q^q \, \mathcal{J}_b \, \mathrm{d}\boldsymbol{\xi} \end{aligned} \tag{14}$$

with the prescribed total stress t_i^{tot} and flux q^q. Moreover, Υ_b denotes a finite element defined on the boundary, e.g., an edge in two-dimensions, with the corresponding reference element $\widehat{\Upsilon}_b$. The subscript $()_\Gamma$ identifies the shape function to be defined on the boundary, hence, defined on

the element $\widehat{\Upsilon}_b$. The whole system written in matrix notation reads as

$$\begin{bmatrix} \mathbf{M1} & \mathbf{0} \\ \mathbf{M2} & \mathbf{0} \end{bmatrix} \begin{bmatrix} \ddot{\mathbf{u}} \\ \ddot{\mathbf{p}} \end{bmatrix} + \begin{bmatrix} \mathbf{0} & \mathbf{0} \\ \mathbf{C} & \mathbf{P} \end{bmatrix} \begin{bmatrix} \dot{\mathbf{u}} \\ \dot{\mathbf{p}} \end{bmatrix} + \begin{bmatrix} \mathbf{K} & -\mathbf{G1} \\ \mathbf{0} & \mathbf{G2} \end{bmatrix} \begin{bmatrix} \mathbf{u} \\ \mathbf{p} \end{bmatrix} = \begin{bmatrix} \mathbf{f}^u \\ \mathbf{f}^p \end{bmatrix}.$$

It must be mentioned that in the definition of the single components (13) and (14) of the algebraic equation system no Dirichlet boundary conditions are considered. Thus, the boundary conditions have to be considered in a later step. There exists several methods and a good overview is given in the book of Jung and Langer [30]. In order to derive the finite element formulation for the Laplace transformed equations (3) basically the same steps have to be performed. Since this procedure is straight forward this derivation will be skipped here for simplicity.

4 Infinite element for poroelastodynamics

Infinite elements have to be constructed in such a way that they represent unbounded domains in an appropriate manner. Thus, in unbounded domains they have to transfer outward traveling waves to infinity. They also have to ensure that no incoming waves will appear as long as there is no source in the far field. In the three-dimensional case, the existence of multiple waves has to be considered. In a semi-infinite halfspace three different wave types are observable as revealed in section 2.2. In the following, an infinite element will be presented which is capable to fulfill this requirements properly.

4.1 Geometric discretization

The geometry of an infinite element, which follows mainly the proposed infinite element of Astley et al. [5], for the three-dimensional case is depicted in figure 1. The set containing the

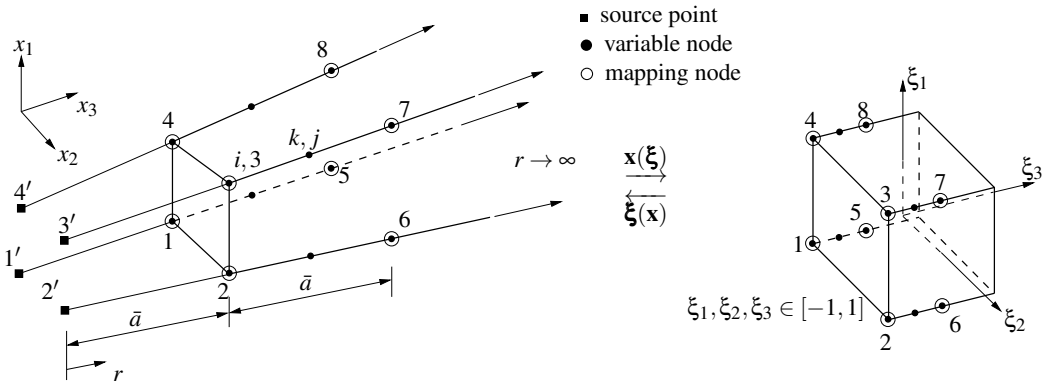

(a) Infinite element in physical space

(b) Corresponding mapped element in local coordinates

Figure 1: Three-dimensional infinite element

points on the base face (x_1x_2-plane) is defined with $n_B = \{1, 2, \ldots, n_B^P\}$, where n_B^P denotes the

number of base points for the approximation of the field quantity (e.g., $n_B^P = 4$, as it is depicted in figure 1). Thus, the infinite element isn't restricted to a linear approximation order on the base face. The radial direction of the infinite element is defined by the so called source points which are defined by the set $n_S = \{1', 2', \ldots, (n_B^P)'\}$. Source points denote locations, where the load is applied and may collapse to a single point. Consequently, the radial direction of the infinite element is given through corresponding source and base points (see figure 1(a)) as well through radial distances a_i, with $i \in n_B$. In any case, it must be ensured that the source points for every infinite element are chosen in such a way that the single infinite elements do not intersect each other. This is of course ensured when the source point is chosen to be the same for every infinite element. Moreover, the radial directions also lead to the mapping points $n_M = \{n_B^P + 1, \ldots, 2n_B^P\}$, i.e., in the special case of figure 1, $n_M = \{5,6,7,8\}$. These mapping points are located deliberately at related distances a_i measured from the base points n_B. The distance between points n_M and n_B need not be chosen to be equal to the related radial distances a_i. However, in many physical problems, the source point is often a singular point, from which on the field quantity decays. This behavior can only be represented by the proposed infinite element, if the distances between the related points n_M and n_B is chosen to be equal to a_i. The mapping from the physical to the local space is independent of the approximation order of the field quantity. In radial direction the mapping is performed in such a manner that a $1/r$-like mapping is obtained, viz., the radial mapping functions are defined as

$$\mathsf{m}^1(\xi_3) = \frac{-2\xi_3}{1-\xi_3} \quad , \quad \mathsf{m}^2(\xi_3) = \frac{1+\xi_3}{1-\xi_3} \, .$$

The mapping on the base face uses conventional finite element shape functions, denoted by $S^i(\xi_1, \xi_2)$, with $i \in n_B$. The geometric mapping from the physical to the local space is defined by

$$\mathbf{x}(\boldsymbol{\xi}) = \mathsf{m}^1(\xi_3) \sum_{i=1}^{n_B^P} S^i(\xi_1, \xi_2) \mathbf{p}^i + \mathsf{m}^2(\xi_3) \sum_{i=1}^{n_B^P} S^i(\xi_1, \xi_2) \mathbf{p}^{i+n_B^P} \, , \tag{15}$$

where $\mathbf{p}^i$ denotes geometrical points of the infinite element [37]. The above mapping functions (15) assure the compatibility condition at the base nodes between the infinite and conventional finite elements. The relation between the radial distance measure r and the local coordinate is given by

$$\xi_3 = 1 - \frac{2\bar{a}}{r} \quad , \quad r - \bar{a} = \bar{a} \frac{1+\xi_3}{1-\xi_3} \, .$$

Thus, the proposed relation maps points located at $r \to \infty$ to $\xi_3 = +1$ in the local element. Moreover, the introduced distance $\bar{a}$ is defined as

$$\bar{a} = \frac{1}{n_B^P} \sum_{i=1}^{n_B^P} a_i$$

and will be referred in the following as characteristic length of the infinite element.

4.2 Shape function

The wave behavior of the far field in a poroelastic medium can be approximately represented in Laplace domain by exponential functions. This is due to the fact that the waves in the far field can be approximately represented by the superposition of plane waves [58, 41, 28].

Nevertheless, attention must be paid to the question which type of constituent is able to transfer which type of wave, since multiple waves are present in a three-dimensional problem. In an unbounded three-dimensional poroelastic medium two compressional waves and a shear wave may be present with wave velocities c_1, c_2 and c_S, respectively, as discussed in section 2.2. In a halfspace, additionally, the Rayleigh wave can be observed [44]. Whereas both compressional waves, with wave speeds c_1 and c_2, are transferred by the solid displacement and the pore pressure, the shear and consequently, the Rayleigh wave with wave speeds c_S and c_R, can be transferred only by the solid displacement. Thus, the shape and test function of the solid displacement u_i is defined as

$$\varphi^j(\boldsymbol{\xi}) = \frac{(1-\xi_3)}{2} S^i(\xi_1,\xi_2) P_p^k(\xi_3) \frac{1}{3} \left(\left[U_1^{\mathrm{K}} \mathrm{e}^{-\frac{s}{c_1}\mu(\bar{a},\xi_3)} + U_2^{\mathrm{K}} \mathrm{e}^{-\frac{s}{c_2}\mu(\bar{a},\xi_3)} \right] + \mathrm{e}^{-\frac{s}{c_S}\mu(\bar{a},\xi_3)} + \mathrm{e}^{-\frac{s}{c_R}\mu(\bar{a},\xi_3)} \right) \tag{16}$$

and the shape function for the fluid pore pressure reads as

$$\vartheta^j(\boldsymbol{\xi}) = \frac{(1-\xi_3)}{2} S^i(\xi_1,\xi_2) P_p^k(\xi_3) \left[P_1^{\mathrm{K}} \mathrm{e}^{-\frac{s}{c_1}\mu(\bar{a},\xi_3)} + P_2^{\mathrm{K}} \mathrm{e}^{-\frac{s}{c_2}\mu(\bar{a},\xi_3)} \right]. \tag{17}$$

The parameters $U_i^{\mathrm{K}}, P_i^{\mathrm{K}}$, with $i = 1,2$, are a kind of wave weighting factors. In other words the two compressional waves c_1 and c_2 are related to each other, which is modeled by the mentioned weighting factors. These factors can be determined by the one-dimensional analytical solution of a poroelastic rod [31, 32] and, hence, are only an approximation for the application in three-dimensional problems. The most meaningful property of these weighting factors is that their sum is equal to one, i.e.,

$$U_1^{\mathrm{K}} + U_2^{\mathrm{K}} = 1 \,, \qquad P_1^{\mathrm{K}} + P_2^{\mathrm{K}} = 1 \,.$$

Following the work of Khalili et al. [31], the wave weighting factors are defined in $1D$ as

$$U_1^{\mathrm{K}} = \frac{C_3 v_1^3 \mathrm{e}^{-s\lambda_1\bar{a}}}{C_3 v_1^3 \mathrm{e}^{-s\lambda_1\bar{a}} + C_4 v_1^4 \mathrm{e}^{-s\lambda_2\bar{a}}} \quad , \qquad U_2^{\mathrm{K}} = \frac{C_3 v_1^3 \mathrm{e}^{-s\lambda_2\bar{a}}}{C_3 v_1^3 \mathrm{e}^{-s\lambda_1\bar{a}} + C_4 v_1^4 \mathrm{e}^{-s\lambda_2\bar{a}}} \,,$$

$$P_1^{\mathrm{K}} = \frac{C_3 v_2^3 \mathrm{e}^{-s\lambda_1\bar{a}}}{C_3 v_2^3 \mathrm{e}^{-s\lambda_1\bar{a}} + C_4 v_2^4 \mathrm{e}^{-s\lambda_2\bar{a}}} \quad , \qquad P_2^{\mathrm{K}} = \frac{C_3 v_2^3 \mathrm{e}^{-s\lambda_2\bar{a}}}{C_3 v_2^3 \mathrm{e}^{-s\lambda_1\bar{a}} + C_4 v_2^4 \mathrm{e}^{-s\lambda_2\bar{a}}} \,.$$

where the superscript K of the wave weighting factors denotes the affinity to the Khalili infinite element. The coefficients v_1^i and v_2^i, with $i = 3,4$, are obtained from the analytical one-dimensional solution and are defined in (29). It remains to define the yet unknown constants C_3 and C_4. This can be accomplished by defining problem specific boundary conditions in dependence of the given problem, as shown by Khalili [31]. Moreover, the phase term $\mu(\bar{a},\xi_3)$ is introduced. The phase term consists of the distance $\bar{a}$ and a radial weight

$$\mu(\bar{a},\xi_3) = \bar{a}\frac{1+\xi_3}{1-\xi_3} \,.$$

Note that the geometric factor is equal to the mapping function $\mathsf{m}^2(\xi_3)$. Thus, the phase-like term vanishes at $\xi_3 = -1$ and approaches the distance $\bar{a}$ for $\xi_3 = 0$. The exponential factors in (16) and (17) represents, therefore, a radial wave-like factor of the form $\exp(\frac{s}{c}(r-\bar{a}))$ within each element [5].

The radial approximation is done by a polynomial function $P_p^k(\xi_3)$ of order p. The superscript $k \in \{1,\ldots,p+1\}$ denotes the corresponding radial node the polynomial belongs to. The approximation order depends on the number of nodes located within the mapping points n_B and n_M. Furthermore, equally spaced nodes within the interval $\xi_3 \in [-1,0]$ are assumed for the construction of the polynomials $P_p^k(\xi_3)$. In general, the most intuitive way to construct the radial interpolation polynomial is the use of the well known *Lagrange polynomials*. The optimal choice of interpolation functions was investigated by Dreyer et al. [24] for the acoustic case. Dreyer recommends for problems of exterior acoustics the use of *Jacobi polynomials*, which will result in better conditioned system matrices. Consequently, the radial interpolation functions are constructed by using Jacobi polynomials, as suggested by Dreyer et al. [23], if not otherwise stated. Jacobi polynomials are generalized *Legendre polynomials* and are defined by

$$P_{(\alpha,\beta)}^k(\xi_3) = \frac{(-1)^k}{2^k!k}(1-\xi_3)^{-\alpha}(1+\xi_3)^{-\beta}\frac{\mathrm{d}^k}{\mathrm{d}\xi_3^k}\left[(1-\xi_3)^{\alpha+k}(1+\xi_3)^{\beta+k}\right] .$$

These polynomials are *orthogonal polynomials* and satisfy therefore the relation

$$\int_{-1}^{+1} P_{(\alpha,\beta)}^i P_{(\alpha,\beta)}^j (1-\xi_3)^{\alpha}(1+\xi_3)^{\beta}\,\mathrm{d}\xi_3 = \chi(\alpha,\beta,j)\delta_{ij} ,$$

where $\chi(\alpha,\beta,j)$ is a function depending on the parameters α,β, and j. To ensure compatibility between the finite and infinite elements at their interface, the interpolation condition $\varphi^i(\mathbf{x}_j) = \delta_{ij}$ has to be fulfilled. However, Jacobi polynomials don't automatically satisfy this interpolation condition. Thus, the first polynomial within the portion of radial shape functions $p+1$ has to fulfill $P_p^1(-1) = 1$, whereas all other polynomials have to satisfy $P_p^i(-1) = 0$, with $1 < i \leq p+1$. This can easily be obtained by applying adequate constant shifts of the single polynomials. The index j is a function of the base node numbering i and the radial node numbering k

$$j(k,i) \quad , \quad i \in n_B \quad , \quad 1 \leq k \leq p+1 \quad , \quad 1 \leq j \leq (p+1)n_B^P .$$

The factor $\frac{1}{2}(1-\xi_3)$ in equation (16) ensures that no constant terms remain in the shape functions $\varphi^j(\boldsymbol{\xi})$ and ensures the shape functions to vanish at infinity, i.e., $\varphi^j(\boldsymbol{\xi}) \to 0$ as $\xi_3 \to +1$. Moreover, the Sommerfeld radiation condition is approximated. Thus, when considering a radial approximation polynomial of the form

$$P_p(\xi_3) = c_0 + c_1\xi_3 + c_2\xi_3^2 + \cdots + c_p\xi_3^p ,$$

the behavior of the shape functions $\varphi^j(\boldsymbol{\xi})$ in radial direction is, when ξ_1 and ξ_2 are held constant

$$\varphi^j \approx \left[\frac{\gamma_1}{r} + \frac{\gamma_2}{r^2} + \cdots + \frac{\gamma_p}{r^p}\right]\left(\left[\hat{U}_1^{\mathrm{K}}\,\mathrm{e}^{-\frac{s}{c_1}\mu(\bar{a},\xi_3)} + \hat{U}_2^{\mathrm{K}}\,\mathrm{e}^{-\frac{s}{c_2}\mu(\bar{a},\xi_3)}\right] + \mathrm{e}^{-\frac{s}{c_S}\mu(\bar{a},\xi_3)} + \mathrm{e}^{-\frac{s}{c_R}\mu(\bar{a},\xi_3)}\right),$$

where c_i and γ_i denote constants.

It remains to select the test function for the solid displacement and the pore pressure, which are defined as

$$\bar{\varphi}^j(\boldsymbol{\xi}) = D(\xi_3)\varphi^j(\boldsymbol{\xi}) \,, \qquad \bar{\vartheta}^j(\boldsymbol{\xi}) = D(\xi_3)\vartheta^j(\boldsymbol{\xi}) \,,$$

and differ from the ansatz function only by the additional weight

$$D(\xi_3) = \frac{(1-\xi_3)^2}{4} \,.$$

The additional weight $D(\xi_3)$ ensures finiteness of integrals occurring in the discrete variational formulation. Thus, the need of square integrability is fulfilled. Even more, the test function fulfills the interpolation condition, which preserves a compatible matching of finite and infinite elements at their interface.

4.3 1D infinite element

The above defined three-dimensional shape function for the solid phase (16) can be condensed to the one-dimensional case yielding

$$\varphi^j(\xi_3) = P_p^k(\xi_3) \left[\hat{U}_1^{\mathrm{K}} \, \mathrm{e}^{-\frac{s}{c_1}\mu(\bar{a},\xi_3)} + \hat{U}_2^{\mathrm{K}} \, \mathrm{e}^{-\frac{s}{c_2}\mu(\bar{a},\xi_3)} \right] . \tag{18}$$

Note that the term $\frac{1}{2}(1-\xi_3)$ also vanished, since in the one-dimensional case no static solution has to be obtained. Applying the same procedure to (17) yields the shape function for the fluid pore pressure

$$\vartheta^j(\xi_3) = P_p^k(\xi_3) \left[\hat{P}_1^{\mathrm{K}} \, \mathrm{e}^{-\frac{s}{c_1}\mu(\bar{a},\xi_3)} + \hat{P}_2^{\mathrm{K}} \, \mathrm{e}^{-\frac{s}{c_2}\mu(\bar{a},\xi_3)} \right] . \tag{19}$$

4.4 Simplified approach of shape functions

The simplified model is based on the fact that the slow (or second) wave in a poroelastic material is highly damped and thus, for realistic most common poroelastic materials, not observable [44]. In this case it is reasonable to neglect the influence of the slow wave and to approximate only the fast (or first) compressional wave. This corresponds to the case that the wave weighting factors approach $\hat{U}_1^{\mathrm{K}} = \hat{P}_1^{\mathrm{K}} \approx 1$, whereas $\hat{U}_2^{\mathrm{K}} = \hat{P}_2^{\mathrm{K}} \approx 0$. Thus, the simplified shape and test functions of the infinite element for the three dimensional case are defined as

$$\begin{aligned} \varphi^j(\boldsymbol{\xi}) &= \frac{1}{2}(1-\xi_3) S^i(\xi_1,\xi_2) P_p^k(\xi_3) \frac{1}{3} \left(\mathrm{e}^{-\frac{s}{c_1}\mu(\bar{a},\xi_3)} + \mathrm{e}^{-\frac{s}{c_S}\mu(\bar{a},\xi_3)} + \mathrm{e}^{-\frac{s}{c_R}\mu(\bar{a},\xi_3)} \right) \\ \vartheta^j(\boldsymbol{\xi}) &= \frac{1}{2}(1-\xi_3) S^i(\xi_1,\xi_2) P_p^k(\xi_3) \, \mathrm{e}^{-\frac{s}{c_1}\mu(\bar{a},\xi_3)} \end{aligned} \tag{20}$$

for the solid displacement and the pore pressure, respectively. Of course, this simplified approach is also applicable to the one-dimensional shape functions defined in (18) and (19).

5 Numerical integration

During the evaluation of the infinite element matrices, based on the shape functions of section 4, integrals of the form

$$\int_{-1}^{+1} f(\xi_3)\, \mathrm{e}^{-z\frac{1+\xi_3}{1-\xi_3}}\, \mathrm{d}\xi_3 \tag{21}$$

have to be calculated. In equation (21), $z \in \mathbb{C}$ represent a Complex parameter, e.g., $z = \bar{a}\frac{s}{c}$. The finiteness of the integral is ensured, since the real part of the Laplace parameter is positive by definition, i.e., $\mathrm{Re}(s) > 0$ [22]. It can be verified that also the real part of the fraction s/c is always larger than zero. In order to evaluate this integrals numerically, a Newton-Cotes type formula will be derived. Thus, integration points are chosen and corresponding integration weights are calculated. To explain the integration procedure a two point integration rule will be derived. The chosen points are for example

$$\xi_3^1 = -\tfrac{1}{3}\ , \quad \xi_3^2 = +\tfrac{1}{3}\ .$$

The polynomial $f(\xi_3)$ is approximated by Lagrange polynomials P_p^k, with $p = 1$ and $k = 1,2$, and is, therefore, expressed as

$$f(\xi_3) = f^1 P_1^1(\xi_3) + f^2 P_1^2(\xi_3)\ ,$$

where $f^1 = f(\xi_3^1)$ and $f^2 = f(\xi_3^2)$ are the values of $f(\xi_3^k)$ evaluated at the integration points. Thus, the given integral (21) can be rewritten

$$\begin{aligned}\int_{-1}^{+1} f(\xi_3)\, \mathrm{e}^{-z\frac{1+\xi_3}{1-\xi_3}}\, \mathrm{d}\xi_3 &= f^1 \int_{-1}^{+1} P_1^1(\xi_3)\, \mathrm{e}^{-z\frac{1+\xi_3}{1-\xi_3}}\, \mathrm{d}\xi_3 + f^2 \int_{-1}^{+1} P_1^2(\xi_3)\, \mathrm{e}^{-z\frac{1+\xi_3}{1-\xi_3}}\, \mathrm{d}\xi_3 \\ &= f^1 w^1 + f^2 w^2\ ,\end{aligned}$$

with the integrations weights w^1 and w^2, defined by the integrals. During the derivation of the integration weights, integrals of the product of the single monomials with the exponential term must be performed, yielding

$$\int_{-1}^{+1} (\xi_3)^0\, \mathrm{e}^{-z\frac{1+\xi_3}{1-\xi_3}}\, \mathrm{d}\xi_3 = 2 + 2z\,\mathrm{e}^z \left(\mathrm{Ei}(-z) + \frac{1}{2}\left(\log(-\tfrac{1}{z}) - \log(\tfrac{1}{z}) - \log(-z) + \log(z) \right) \right)$$

$$\int_{-1}^{+1} (\xi_3)^1\, \mathrm{e}^{-z\frac{1+\xi_3}{1-\xi_3}}\, \mathrm{d}\xi_3 =$$

$$2z \left[1 + (1+z)\,\mathrm{e}^z \left(\mathrm{Ei}(-z) + \frac{1}{2}\left(\log(-\tfrac{1}{z}) - \log(\tfrac{1}{z}) - \log(-z) + \log(z) \right) \right) \right]\ ,$$

where $\mathrm{Ei}(-z)$ denotes the *Exponential Integral* [52]. Consequently, the integration weights results in

$$\begin{aligned} w^1 &= 1-3z-z(2+3z)\,\mathrm{e}^z\left(\mathrm{Ei}(-z)+\frac{1}{2}\left(\log(-\tfrac{1}{z})-\log(\tfrac{1}{z})-\log(-z)+\log(z)\right)\right) \\ w^2 &= 1+3z+z(4+3z)\,\mathrm{e}^z\left(\mathrm{Ei}(-z)+\frac{1}{2}\left(\log(-\tfrac{1}{z})-\log(\tfrac{1}{z})-\log(-z)+\log(z)\right)\right). \end{aligned} \tag{22}$$

The proposed integration rule is exact for polynomials of degree $m-1$, when m is the number of integration points. Note that the integration weights are frequency dependent, whereas the integration points remain to be real valued. Thus, the integration weights have to be recalculated for every needed frequency.

The integration on the base face of the infinite element in figure 1 is still performed with the standard *Gauß quadrature*, whereas the integral of the infinite direction is evaluated using the above derived integration rule.

5.1 Efficient evaluation of integration weights

A crucial point in the evaluation of the integration weights of the integral (21) is the computation of the Exponential Integral $\mathrm{Ei}(-z)$. Different approaches are possible to evaluate this integral. Actually, the calculation is divided into three ranges of values of z, namely

- $(\mathrm{Re}(z)<5)\wedge(\mathrm{Abs}(\mathrm{Im}(z))<5)$: An efficient way of computing the Exponential Integral is proposed by Amos [2]. The FORTRAN subroutine supplied by Amos [1] is used.
- $(5\leq\mathrm{Re}(z)<100)\wedge(5\leq\mathrm{Abs}(\mathrm{Im}(z))<100)$: The integration weights are calculated by interpolation from pre-calculated look-up tables. These look-up tables were generated using the software package Mathematica [53].
- $(\mathrm{Re}(z)\geq 100)\vee(\mathrm{Abs}(\mathrm{Im}(z))\geq 100)$: For values of $z\to\infty$ the asymptotic series expansion

$$\mathrm{Ei}(-z)\approx-\frac{\mathrm{e}^{-z}}{z}\sum_{k=0}^{\infty}\frac{k!}{(-z)^k}-\frac{1}{2}\left(\log(-\tfrac{1}{z})-\log(\tfrac{1}{z})-\log(-z)+\log(z)\right)$$

  is valid [52]. Inserting the above asymptotic series expansion into the weights (22) yields

$$\begin{aligned} w^1 &= 1-3z-z(2+3z)\left(-\frac{1}{z}\sum_{k=0}^{\infty}\frac{k!}{(-z)^k}\right)=\frac{4}{z}-\frac{14}{z^2}+\frac{60}{z^3}-\frac{312}{z^4}+\dots \\ w^2 &= 1+3z+z(4+3z)\left(-\frac{1}{z}\sum_{k=0}^{\infty}\frac{k!}{(-z)^k}\right)=-\frac{2}{z}+\frac{10}{z^2}-\frac{48}{z^3}+\frac{264}{z^4}-\dots\,. \end{aligned}$$

  Note that the above weights aren't equal, although the integration points are symmetric. The series expansion is truncated after a precision of at least eight digits is obtained. This is ensured by a comparison of the weights calculated with the above series expansion and exact calculated weights (22) using the computing package Mathematica [53]. For example, for a five point integration rule, twelve terms of the series expansion are used.

6 Time domain solution of coupled finite and infinite elements

When using the finite element method to model bounded physical problems, the temporal discretization is accomplished by using a numerical time stepping scheme, e.g., the Newmark method [40]. When dealing with unbounded domains a special treatment is necessary. The Newmark algorithm can't be used as time stepping scheme in dynamic problems with infinite elements, because the shape functions of the infinite elements are non-local in time. This is due to the fact that the shape functions of the infinite elements are constructed in Laplace domain to provide the wave behavior (cf. section 4). In order to obtain a time domain solution an inverse Laplace transformation is needed. A method which serves this aim is the convolution quadrature method (CQM) [44]. This brings up the idea to combine these two time stepping methods. Thus, the Newmark method will be applied to the time integration of the near field, whereas the time domain solution of the far field will be calculated using the CQM. This purpose can be accomplished by using the *substructure method* or *domain decomposition method*.

The application of the proposed substructure method is explained in the following. Consider a discretized domain $\overline{\Omega}_h = \Omega_h \cup \Gamma$ with the corresponding boundary Γ. The domain Ω_h is decomposed into two non-overlapping subdomains.

$$\Omega_h = \Omega_h^{\mathrm{NEW}} \cup \Omega_h^{\mathrm{CQM}} \,, \quad \Omega_h^{\mathrm{NEW}} \cap \Omega_h^{\mathrm{CQM}} = \varnothing \,, \tag{23}$$

as shown in figure 2. The same procedure has to be applied to the Dirichlet- Γ_{D} and Neumann boundary Γ_{N} ($\Gamma = \Gamma_{\mathsf{D}} \cup \Gamma_{\mathsf{N}}$). In equation (23), Ω^{NEW} and Ω^{CQM} denote the subdomains where

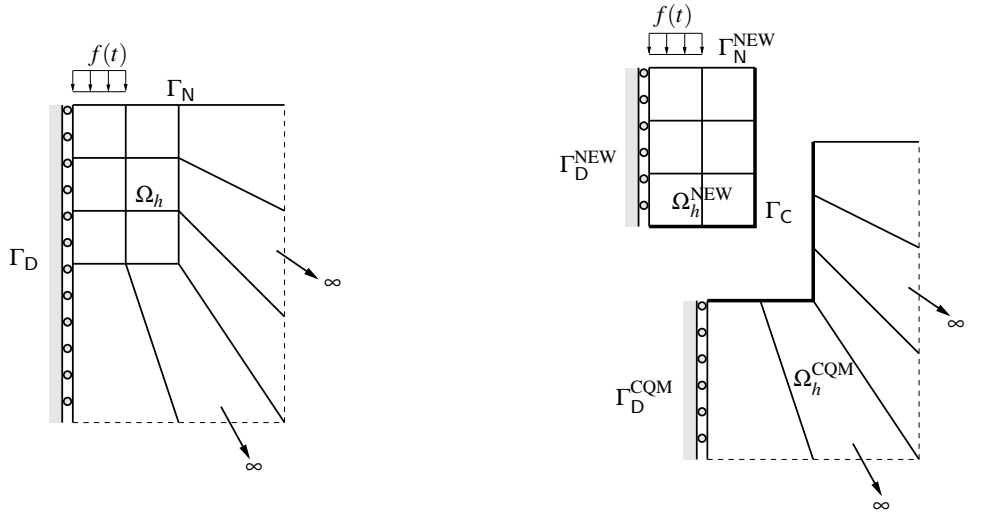

(a) Single domain (b) Decomposition into two subdomains

Figure 2: Decomposition of the domain Ω_h into near Ω_h^{NEW} and far field Ω_h^{CQM}

the Newmark integration scheme and the convolution quadrature method, respectively, is applied to obtain the time domain solution. Due to the subdivision

$$\Gamma_{\mathsf{C}} = \overline{\Omega}^{\mathrm{NEW}} \cap \overline{\Omega}^{\mathrm{CQM}}$$

the *interface* Γ_{C} is generated. Moreover, to maintain a well posed equation system so called *interface conditions* (continuity of solid displacement and pore pressure as well as the equilibrium of the total stress and the flux) have to be formulated. A node by node coupling of the two domains is used to fulfill these conditions.

In order to illustrate the coupling process the equation systems of the single subdomains are reordered according to degrees of freedom belonging to the interior or the interface of the subdomains. Thus, the resulting equation system of the Newmark method for the time step n

$$\overline{\mathbf{K}}\mathbf{u}_n = \mathbf{f}_n + \mathbf{r}_n$$

of domain $\overline{\Omega}^{\mathrm{NEW}}$ is decomposed as

$$\begin{bmatrix} \overline{\mathbf{K}}_{\mathsf{II}}^{\mathrm{NEW}} & \overline{\mathbf{K}}_{\mathsf{IC}}^{\mathrm{NEW}} \\ \overline{\mathbf{K}}_{\mathsf{CI}}^{\mathrm{NEW}} & \overline{\mathbf{K}}_{\mathsf{CC}}^{\mathrm{NEW}} \end{bmatrix} \begin{bmatrix} (\mathbf{u}_{\mathsf{I}}^{\mathrm{NEW}})_n \\ (\mathbf{u}_{\mathsf{C}}^{\mathrm{NEW}})_n \end{bmatrix} = \begin{bmatrix} (\mathbf{f}_{\mathsf{I}}^{\mathrm{NEW}})_n + (\mathbf{r}_{\mathsf{I}}^{\mathrm{NEW}})_n \\ (\mathbf{f}_{\mathsf{C}}^{\mathrm{NEW}})_n + (\mathbf{r}_{\mathsf{C}}^{\mathrm{NEW}})_n \end{bmatrix} , \tag{24}$$

where the superscripts I and C refer to the interior and interface of each subdomain, respectively. The displacement vector is denoted by $\mathbf{u}_n$, $\overline{\mathbf{K}}$ denotes the resulting system matrix (often called dynamic stiffness matrix), and $\mathbf{r}_n$ is the vector containing the "history" information of the last time step $n-1$. The vector $\mathbf{f}_n$ contains nodal forces.

The convolution

$$\hat{\overline{\mathbf{K}}}(s)\hat{\mathbf{u}}(s) = \hat{\mathbf{f}}(s) \bullet\!\!-\!\!\circ \int_0^t \overline{\mathbf{K}}(t-\tau)\mathbf{u}(\tau)\,\mathrm{d}\tau = \mathbf{f}(t)$$

occurring within the equation system (12) when a infinite element is considered (due to the non-local behavior of the shape functions) can be approximated by the CQM [44] for the time step n as

$$\boldsymbol{\omega}_0\mathbf{u}_n = \mathbf{f}_n - \underbrace{\sum_{k=0}^{n-1} \boldsymbol{\omega}_{n-k}\mathbf{u}_k}_{\mathbf{r}_n} .$$

Here, $\boldsymbol{\omega}_k$ denotes quadrature weights and the vector $\mathbf{r}_n$ contains the history of all previous time steps. Hence, efficiency of this method decreases with an increasing number of time steps. The above equation system of the convolution quadrature is decomposed as

$$\begin{bmatrix} \overline{\boldsymbol{\omega}}_{\mathsf{II}}^{\mathrm{CQM}} & \overline{\boldsymbol{\omega}}_{\mathsf{IC}}^{\mathrm{CQM}} \\ \overline{\boldsymbol{\omega}}_{\mathsf{CI}}^{\mathrm{CQM}} & \overline{\boldsymbol{\omega}}_{\mathsf{CC}}^{\mathrm{CQM}} \end{bmatrix} \begin{bmatrix} (\mathbf{u}_{\mathsf{I}}^{\mathrm{CQM}})_n \\ (\mathbf{u}_{\mathsf{C}}^{\mathrm{CQM}})_n \end{bmatrix} = \begin{bmatrix} (\mathbf{f}_{\mathsf{I}}^{\mathrm{CQM}})_n + (\mathbf{r}_{\mathsf{I}}^{\mathrm{CQM}})_n \\ (\mathbf{f}_{\mathsf{C}}^{\mathrm{CQM}})_n + (\mathbf{r}_{\mathsf{C}}^{\mathrm{CQM}})_n \end{bmatrix} , \tag{25}$$

where the coefficient matrix $\boldsymbol{\omega}_0$ is replaced by $\overline{\boldsymbol{\omega}}$. The global equation system for time step n is obtained by assembling the equations systems of the subdomains (24) and (25) yielding

$$\underbrace{\begin{bmatrix} \overline{\mathbf{K}}_{\mathsf{II}}^{\mathrm{NEW}} & \overline{\mathbf{K}}_{\mathsf{IC}}^{\mathrm{NEW}} & \mathbf{0} \\ \overline{\mathbf{K}}_{\mathsf{CI}}^{\mathrm{NEW}} & \overline{\mathbf{K}}_{\mathsf{CC}}^{\mathrm{NEW}} + \overline{\boldsymbol{\omega}}_{\mathsf{CC}}^{\mathrm{CQM}} & \overline{\boldsymbol{\omega}}_{\mathsf{CI}}^{\mathrm{CQM}} \\ \mathbf{0} & \overline{\boldsymbol{\omega}}_{\mathsf{IC}}^{\mathrm{CQM}} & \overline{\boldsymbol{\omega}}_{\mathsf{II}}^{\mathrm{CQM}} \end{bmatrix}}_{\mathbf{K}_{\mathrm{sys}}} \begin{bmatrix} (\mathbf{u}_{\mathsf{I}}^{\mathrm{NEW}})_n \\ (\mathbf{u}_{\mathsf{C}})_n \\ (\mathbf{u}_{\mathsf{I}}^{\mathrm{CQM}})_n \end{bmatrix} = \begin{bmatrix} (\mathbf{f}_{\mathsf{I}}^{\mathrm{NEW}})_n + (\mathbf{r}_{\mathsf{I}}^{\mathrm{NEW}})_n \\ (\mathbf{r}_{\mathsf{C}}^{\mathrm{NEW}})_n + (\mathbf{r}_{\mathsf{C}}^{\mathrm{CQM}})_n \\ (\mathbf{f}_{\mathsf{I}}^{\mathrm{CQM}})_n + (\mathbf{r}_{\mathsf{I}}^{\mathrm{CQM}})_n \end{bmatrix} . \tag{26}$$

The resulting global system matrix $\mathbf{K}_{\text{sys}}$ has to be inverted only once, as it is also the case in a pure Newmark equation system or CQM based time stepping scheme. The vector on the right hand side (26) has to be recomputed at every time step for each subdomain, depending on the used time stepping scheme. The application of the suggested method to more than two subdomains can be performed analogously. The time step size of each subdomain is chosen to be equal. But this doesn't need to be necessarily the case [11, 12].

7 Numerical examples

In order to investigate the performance of the proposed infinite element different test examples will be presented. The material data of the considered materials, a soil (coarse sand) and a rock (Berea sandstone), are given in table 1

	$K\ \left[\frac{\text{N}}{\text{m}^2}\right]$	$G\ \left[\frac{\text{N}}{\text{m}^2}\right]$	$\rho\ \left[\frac{\text{kg}}{\text{m}^3}\right]$	$\phi\ [-]$	$K^s\ \left[\frac{\text{N}}{\text{m}^2}\right]$	$\rho_f\ \left[\frac{\text{kg}}{\text{m}^3}\right]$	$K^f\ \left[\frac{\text{N}}{\text{m}^2}\right]$	$\kappa\ \left[\frac{\text{m}^4}{\text{Ns}}\right]$
rock	$8.0 \cdot 10^9$	$6.0 \cdot 10^9$	2458	0.19	$3.6 \cdot 10^{10}$	1000	$3.3 \cdot 10^9$	$1.90 \cdot 10^{-10}$
soil	$2.1 \cdot 10^8$	$9.8 \cdot 10^7$	1884	0.48	$1.1 \cdot 10^{10}$	1000	$3.3 \cdot 10^9$	$3.55 \cdot 10^{-9}$

Table 1: Material data of Berea sandstone (rock) and soil [33]

and are taken from Kim and Kingsbury [33].

7.1 One-dimensional poroelastic rod

First, a one dimensional infinite poroelastic column as depicted in figure 3 will be investigated. It is subjected to a time dependent total stress loading $\sigma^{\text{tot}}(0,t) = 1\,\text{N/m}^2 H(t)$ in terms of a Heaviside step function in time. The boundary condition for the fluid phase is defined by setting the pressure to zero at the top of the column, i.e., $p(0,t) = 0\,\text{N/m}^2$. The near field is discretized

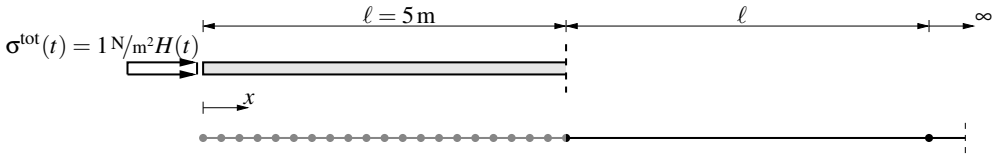

Figure 3: Infinite poroelastic column

with ten quadratic finite elements, whereas the infinite domain is approximated by an one-dimensional infinite element as presented in section 4. Both versions of infinite elements will be used, first, *both compressional waves* are approximated and, second, only the *fast compressional wave* is approximated. The radial approximation polynomial is chosen to be of constant order, i.e., $P_0^k = 1$. In order to validate the performance of the proposed infinite element the solution is compared to the analytic solution given in equation (30). Since, the governing equations (3) are just an *approximation* of the original set of differential equations describing the porous material

[16], also a comparison to results obtained by using the *complete* set of differential equations will be performed. The one-dimensional solution of the poroelastic rod, using Biot's complete theory is given in [45]. Moreover, the solution is compared to results where the far field is represented by the *analytic infinite element* presented in appendix B, whereas the near field is discretized using conventional finite elements.

For simplicity, here, the near and far field is discretized in time by the CQM, which is specified in more detail in [44]. The number of time steps is chosen to be $N = 512$, with time step size $\Delta t = 0.0002\,\mathrm{s}$. In figures 4 and 5, the solid displacement $u(0,t)$ at the top of the column and the pore pressure $p(5,t)$ at the position $x = 5\,\mathrm{m}$ is plotted. The results are denoted by "complete poro" for the calculation when the complete set of differential equations are used and "approx. poro" when the governing equations (3) are used. The calculation using the proposed infinite element is denoted as "FEM-only fast comp. wave (c_1)" when only the fast compressional wave is approximated and as "FEM-both comp. wave (c_1, c_2)" when both compressional waves are approximated. The comparison to the results when the analytic infinite element is attached to the finite element mesh is denoted by "FEM-analytic iFEM". It can be clearly observed that in every plot the different scenarios match each other. Thus, the governing equations (3) represent the behavior of the underlying poroelastic material in an appropriate way, since the results are equal to those of the complete analytic solution. Moreover, it can be noticed that the simplified approximation, where only the fast compressional wave is considered (shape functions (20)), is sufficient. This is obvious by taking a closer look at the wave weighting factors. For the investigated material the wave weighting factors are roughly $\hat{U}_1^{\mathrm{K}} = \hat{P}_1^{\mathrm{K}} \approx 1$ and $\hat{U}_2^{\mathrm{K}} = \hat{P}_2^{\mathrm{K}} \approx 0$. In figures 4(b) and 5(b), the arrival of the first compressional wave can be noticed which lifts the pore pressure within the poroelastic material. Of course, the pore pressure returns back to a equilibrium state $p(x, t \to \infty) = 0$ for an increasing observation time. This is due to the fact that the fluid gains enough time to trickle through the porous material, thus, the pore pressure relaxes with increasing time. Numerical instabilities for large times may occur in the case of soil when the pore pressure is considered and when both compressional waves are approximated as can be noticed in figure 4(b). Consequently, the numerical oscillations are independent on the finite element formulation and may be attributed to the fact that the soil behaves nearly incompressible [46], which results apparently in numerical difficulties.

7.2 Poroelastic halfspace

In the next example a poroelastic halfspace is considered. The underlying material is assumed to be a soil where the material data is given in table 1. A schematic representation of the problem is given in figure 6. The spatial discretization of the near and far field is tested under consideration of the symmetric properties of the problem. Different spatial discretizations are performed and are depicted in figures 7(a)-(c). The near field is discretized with standard 20-noded hexahedron elements (HEX20), whereas the far field is discretized using infinite elements (iFEM). The radial approximation polynomial P_p^k of the infinite elements is chosen to be of first order. Moreover, the calculations using infinite elements (figure 7(a) and 7(b)) are compared to a truncated halfspace which is discretized with conventional finite elements only (see figure 7(c)). The detailed discretization parameters of the near and far field are summarized in table 2.

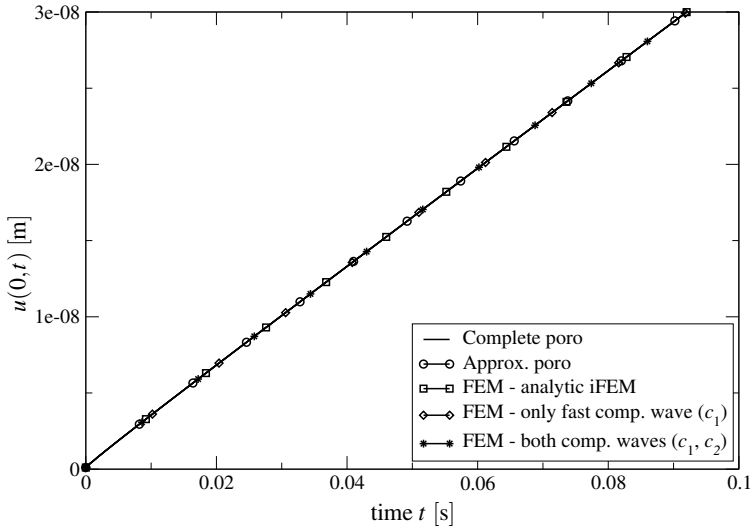

(a) Solid displacement - soil

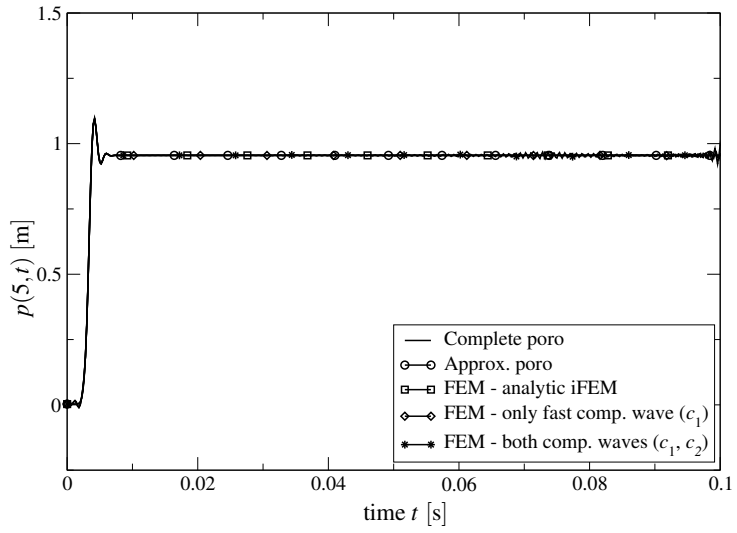

(b) Pore pressure - soil

Figure 4: Infinite poroelastic column - soil

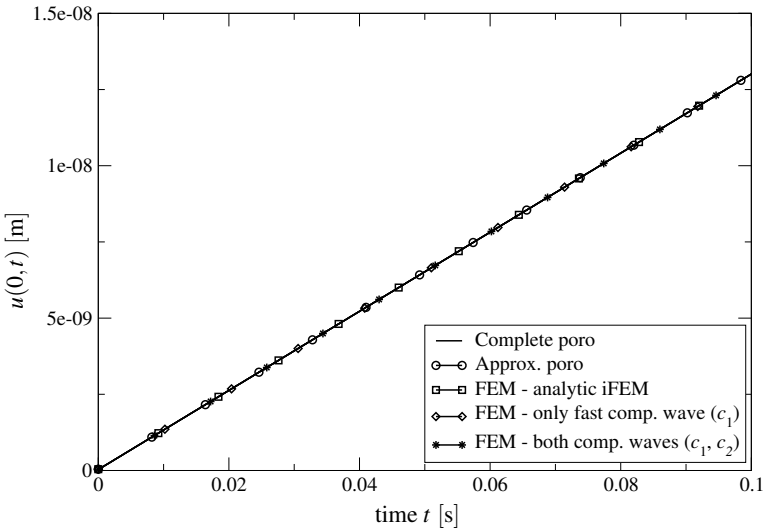

(a) Solid displacement - rock

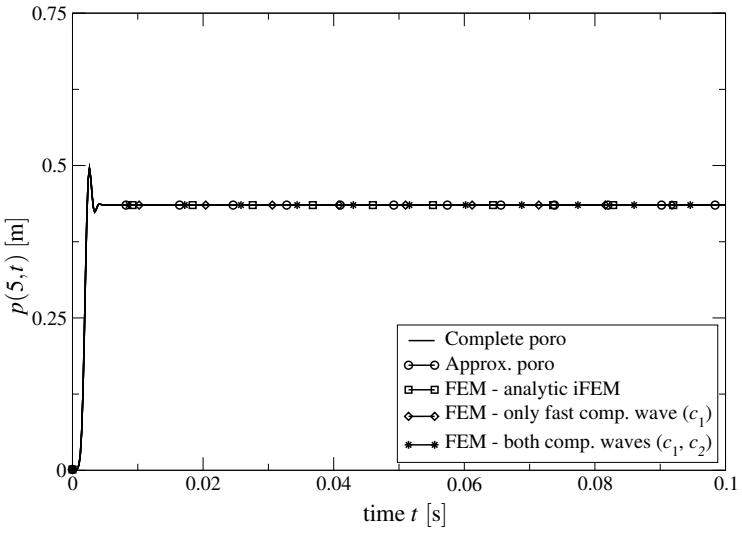

(b) Pore pressure - rock

Figure 5: Infinite poroelastic column - rock

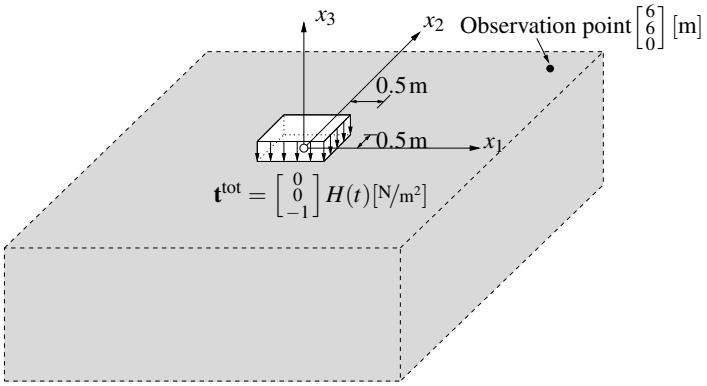

Figure 6: Schematic representation of the poroelastic halfspace

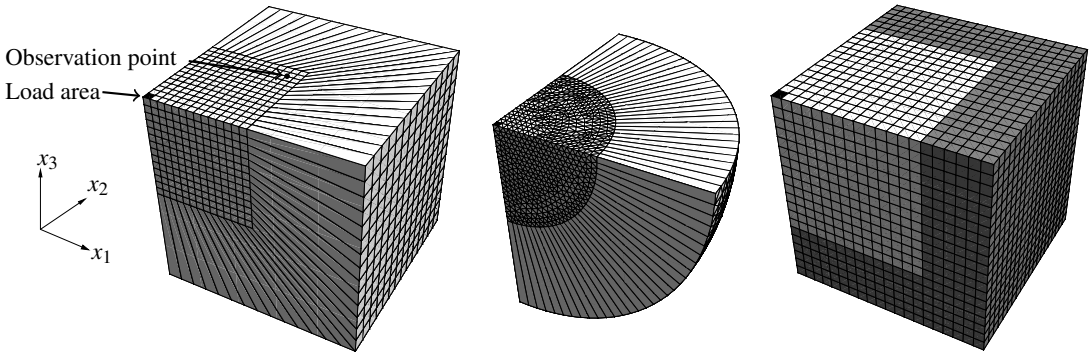

(a) Cube $7\times7\times7\,\text{m}^3$

(b) $1/8$ Sphere $R = 9.7\,\text{m}$

(c) Cube $7\times7\times7\,\text{m}^3$ with attached FEM layer of 3 m thickness

Figure 7: Finite-infinite element discretizations

	Cube $7\times7\times7\,\text{m}^3$	$1/8$ Sphere $R = 9.7\,\text{m}$	Cube $10\times10\times10\,\text{m}^3$
Near field	2744 HEX20	25921 TET10	2744 HEX20
Far field	588 iFEM-FIRST	1330 iFEM-FIRST	5256 HEX20
Loading	$\mathbf{t}^{\text{tot}} = [0\ 0\ -1]^{\text{T}} H(t)[\text{N/m}^2]$ on an area of $0.5\times0.5\,\text{m}^2$		
Observation point	$[6\ 6\ 0]^{\text{T}}\,\text{m}$		
Time step	$\Delta t = 0.0002\,\text{s}$		
Newmark	$\gamma = 0.6$, $\beta = 0.3025$		

Table 2: Time and spatial discretization parameters

The approximation order of the solid displacement and the pore pressure is chosen to be of the same order. The applied load is assumed to be a vertical total stress t_i^{tot} which acts in terms of a Heaviside function in time, i.e., the load is applied and kept constant. The load vector $\mathbf{t}^{\text{tot}} = [0\,0\,-1]^{\text{T}}\,\text{N/m}^2$ is applied on an area of $0.5\times0.5\,\text{m}^2$, whereas the remaining surface is traction free. The pore pressure p is assumed to be zero on the whole surface, i.e., $p(x_1,x_2,0)=0$, and thus assumed to be permeable. On the symmetry planes, the x_1x_3- and x_2x_3-plane, the normal displacements are fixed and also the flux q_i is set to zero. Of course, at infinity the displacements u_i are assumed to be zero as well the pore pressure p. A comparison is also performed to a pure finite element mesh, denoted as "FEM" in the following plots. Here an *additional layer* of 3 m thickness of conventional finite elements is attached as depicted in 7(c). The additional layer is added to attempt to simulate the far field. The bottom is fixed and impermeable, whereas the boundaries to the infinite side are assumed to be free to move and impermeable. Furthermore, vanishing initial conditions are assumed. The time integration is performed using the proposed coupled time stepping scheme presented in section 6. Concerning the Newmark time-stepping scheme the integration parameters γ and β are chosen in such a way that some numerical damping is achieved, as suggested by Zienkiewicz [63] and are given table 2. In order to validate the performance of the proposed infinite element the solid displacements u_i at point $[6\,6\,0]^{\text{T}}\text{m}$ are studied and compared to a BEM calculation [44].

It is of interest to check the theoretical arrival times of the different waves which are present. This can be done, however, only for estimated wave speeds since the wave velocities are frequency dependent (dispersive waves). The wave velocity for the fast compressional wave can be approximated for the special case of $s \to 0$

$$c_1^0 = \sqrt{\frac{\alpha^2 R + \phi^2 (K + \frac{4}{3}G)}{\rho\phi^2}}$$

as suggested in [18]. Hence, the compressional wave speed for the low frequency limit is $c_1^0 = 1690\,\text{m/s}$ for the given soil. The shear wave velocity is for the governing equations (3) already frequency independent and defined in (10) yielding $c_S = 228\,\text{m/s}$. In the following, the Rayleigh wave velocity can be approximated using (11) which results in $c_R = 211\,\text{m/s}$. To calculate the arrival times of the different wave types the distance measure is performed from the outer corner point of the load area, i.e., $[0.5\,0.5\,0]^{\text{T}}\,\text{m}$. They are given in table 3. The arrival times of the different wave types at the observation point are given in column 1. In case if any reflection would take place at the transition from the near to the far field the arrival times at the observation point are given in column 2. Column 3 contains the arrival times from the truncated boundary of the pure finite element mesh.

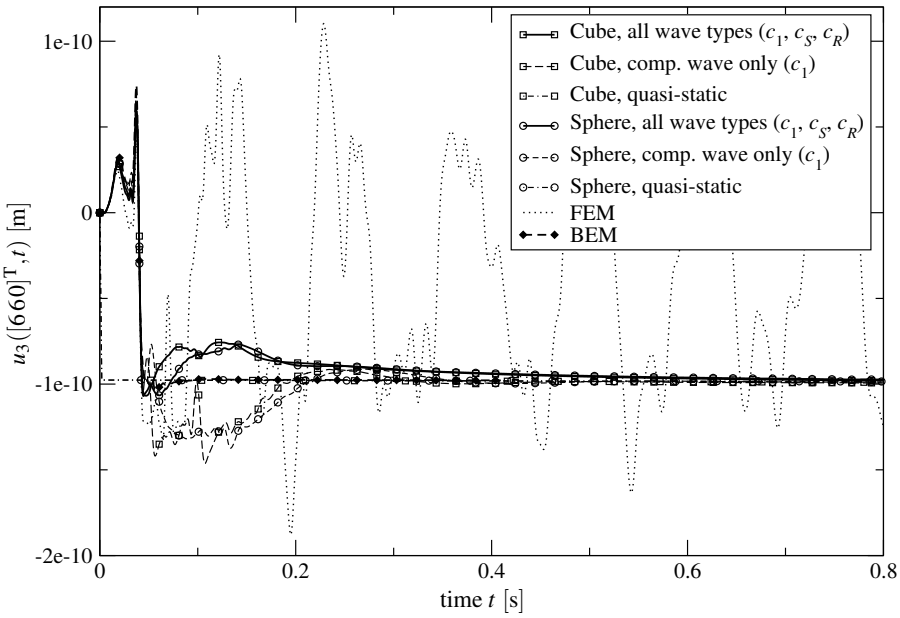

(a) Solid displacement u_3 at observation point $[660]^T$[m] - soil

	Wave speed [m/s]	Distance [m]		
		7.78	9.78	15.78
		Arrival time [s]	Approx. reflection time [s]	
			iFEM	FEM
Comp. wave	1690	0.0046	0.0058	0.0093
Shear wave	228	0.034	0.043	0.069
Rayleigh wave	211	0.037	0.046	0.075

Table 3: Distance measure from load corner point $[0.5\,0.5\,0]^T$ m to observation point with corresponding wave arrival times

The calculation is performed using the presented infinite element, with the shape functions given in (20). Thus, the fast compressional, the shear- and the Rayleigh wave are approximated. The results due to this approximation are denoted by "all wave types (c_1, c_S, c_R)" for the cube- and 1/8 sphere-mesh in figures 8 and 9. The vertical solid displacement u_3 is shown in figure 8(a) and (b), whereas the horizontal solid displacement is depicted in figure 9. These are compared to results of the calculation when only the compressional wave is approximated, denoted by "comp. wave only (c_1)" for the cube- and 1/8 sphere-mesh. Moreover, the results are checked against a "BEM" calculation. It can be observed that all calculations match each other until the compressional wave arrives at the observation point at time $t = 0.0046$s. From this time on the different calculations diverge from each other. This is in a way obvious, since now the infinite elements are activated and the infinite elements which approximate all three wave types possess another behavior as when only one wave is approximated. Furthermore, it can be seen

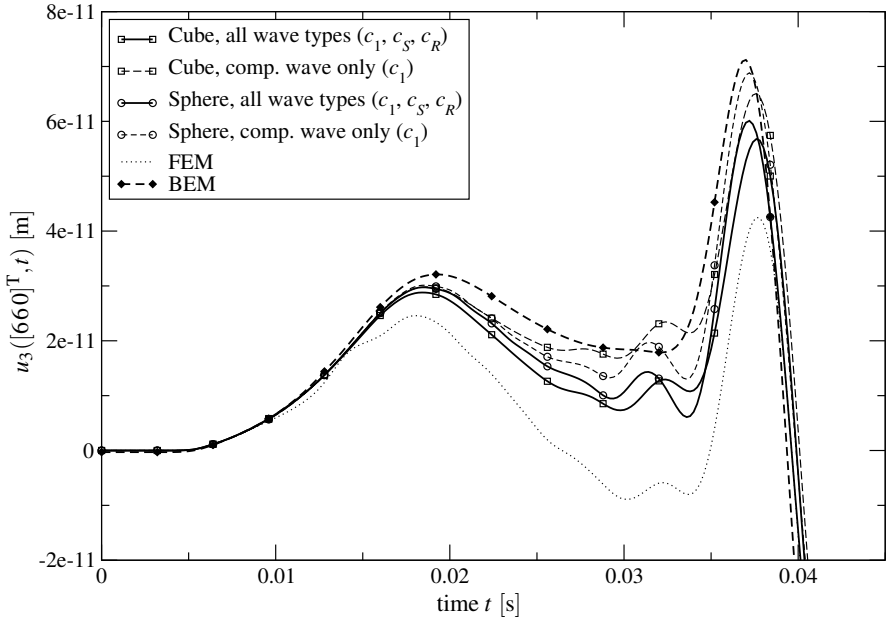

(b) Zoom section of 8(a) - Solid displacement u_3 at observation point $[660]^{\mathrm{T}}$[m] - soil

Figure 8: Vertical solid displacement u_3 at observation point $[660]^{\mathrm{T}}$[m] - soil

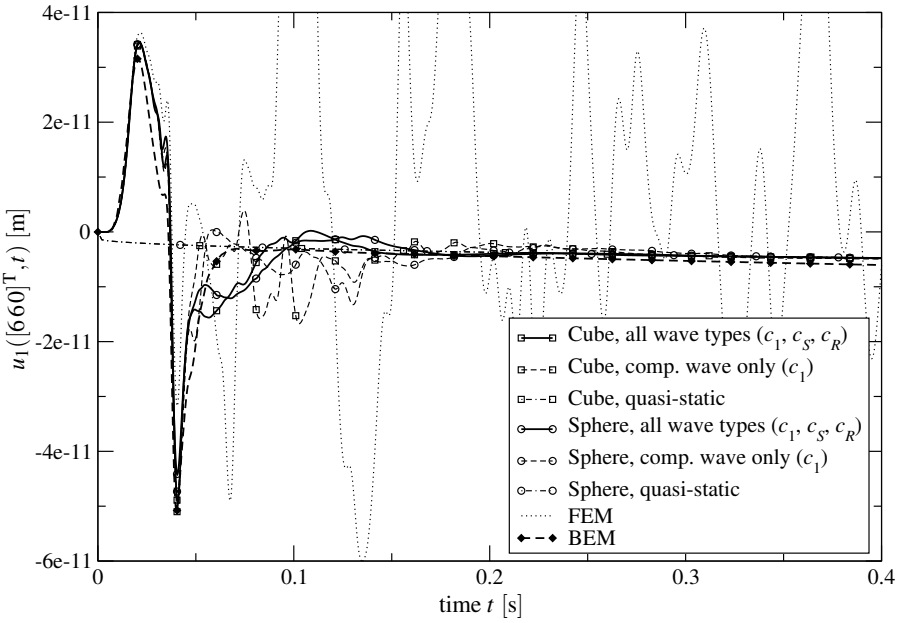

Figure 9: Horizontal solid displacement $u_1 (= u_2)$ at observation point $[660]^{\mathrm{T}}$[m] - soil

that the solution of the pure finite element mesh deviates when the reflected wave from the outer boundary arrives at time $t = 0.0093\,\mathrm{s}$. The Rayleigh pole can also be clearly observed at time $t = 0.037\,\mathrm{s}$ which overlaps with the arrival of the shear wave ($t = 0.034\,\mathrm{s}$). The solutions slightly differ from the BEM calculation which is due to the fact that the infinite elements just can try to approximate the wave behavior of the far field, whereas the BEM fulfills the wave equation exactly within the domain and certainly in infinity. Nevertheless, the results obtained by using the infinite elements are quite good compared to the pure finite element solution. After the waves have passed the observation point the solutions approach the quasi-static solution (denoted by "quasi-static") as can be identified in figures 8(a) and 9. When only the compressional wave is approximated small reflections can be observed compared to the approximation of all wave types. The results of the vertical solid displacement of the cube-mesh are nearly equal as for the $1/8$ sphere-mesh. Consequently, the corner (point $[7\,7\,0]^{\mathrm{T}}\,\mathrm{m}$) of the cube-mesh doesn't affect the solution of the vertical displacement, despite the angle of incidence of the wave isn't normal to the boundary. This conclusion is also confirmed by the horizontal displacement u_1 (figure 7.2), which is equal to u_2 due to the symmtric properties of the problem. Here, the results of the cube-mesh are also nearly the same as for the $1/8$ sphere-mesh. Moreover, the quasi-static solution of any infinite element calculation matches the BEM solution. Compared to the pure finite element calculation the results obtained by using infinite elements are superior and, therefore, approve their necessity.

7.3 Soil on a bedrock

Next, a saturated soil is considered of finite thickness resting on a bedrock, i.e., a poroelastic layer fixed at the bottom. The schematic representation of the problem is sketched in figure 10. The saturated porous layer is assumed to be of 5 m thickness. Below an impermeable bedrock is

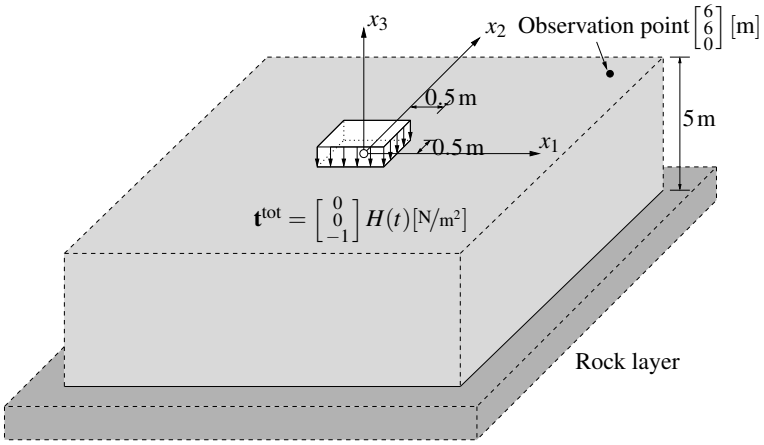

Figure 10: Schematic representation of the poroelastic halfspace resting on a rock layer

assumed, thus, the flux at this boundary and the displacements in any direction are assumed to be zero. The remaining boundary conditions are chosen in the same manner as in the example

before for the pure halfspace. Thus, again the symmetric properties are used. The applied load is given by a vertical total stress $\mathbf{t}^{\text{tot}} = [0\,0\,-1]^{\text{T}}\,\text{N/m}^2$ on an area of $0.5\times0.5\,\text{m}^2$, whereas the remaining portion of the surface is traction free. The spatial discretizations of the near and far field are depicted in figures 11(a) and (b). The radial polynomial P_p^k of the infinite element is chosen to be of first order. The whole discretization parameters are summarized in table 4.

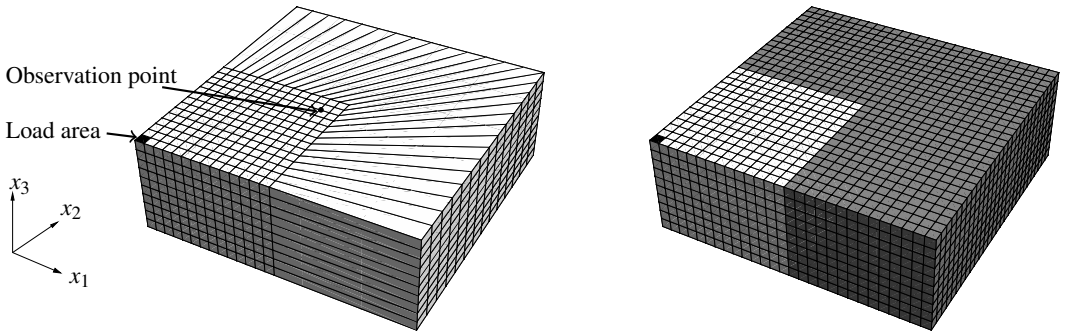

(a) Cube $7\times7\times5\,\text{m}^3$

(b) Cube $7\times7\times5\,\text{m}^3$ with attached pure FEM layer of 7 m thickness

Figure 11: Finite-infinite element discretizations

	Cube $7\times7\times5\,\text{m}^3$	Cube $14\times14\times5\,\text{m}^3$
Near field	1960 HEX20	1960 HEX20
Far field	280 iFEM-FIRST	5880 HEX20
Loading	$t_i^{\text{tot}} = [0\;0\;-1]^{\text{T}} H(t)\,[\text{N/m}^2]$ on an area of $0.5\times0.5\,\text{m}^2$	
Observation point	$[6\;6\;0]^{\text{T}}\,\text{m}$	
Time step	$\Delta t = 0.0002\,\text{s}$	
Newmark	$\gamma = 0.6,\ \beta = 0.3025$	

Table 4: Time and spatial discretization parameters

In order to verify the performance of the proposed infinite element the solid displacement at the observation point $[6\,6\,0]^{\text{T}}\,\text{m}$ is investigated and compared to a BEM calculation [44]. Again, a comparison is performed to a pure finite element mesh, denoted as "FEM" in the following plots. Here, an *additional layer* of 7 m thickness of conventional finite elements is attached as depicted in figure 11(b). The boundaries on the infinite side are assumed to be free to move and impermeable. As in the example before the wave arrival times are inspected as well (see table 5). The distance measure is again performed from the outer corner point of the load area, i.e., $[0.5\,0.5\,0]^{\text{T}}\,\text{m}$. Additionally, the arrival of reflected waves from the rock layer at the observation point will be considered and are listed in column 4.

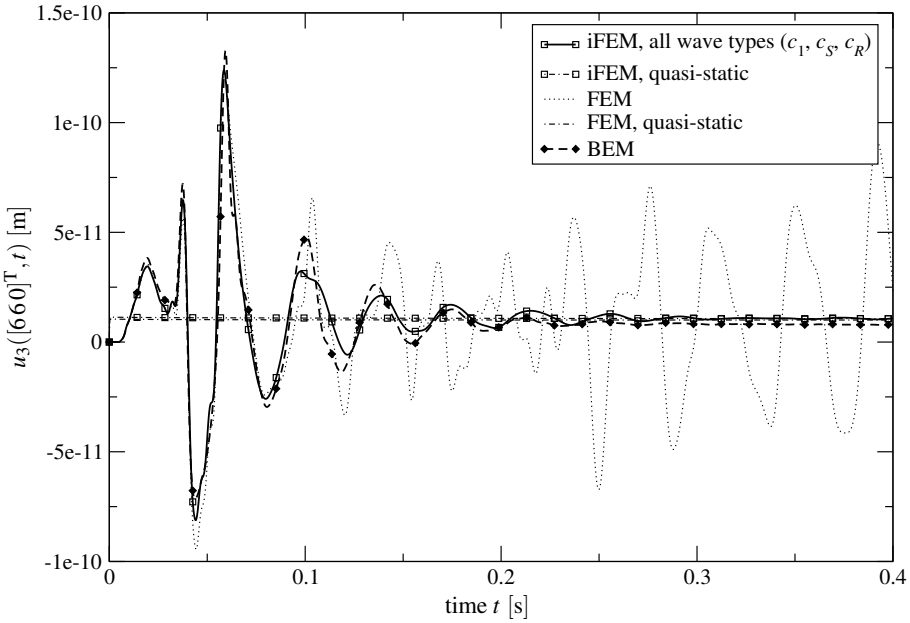

(a) Solid displacement u_3 at observation point $[660]^T$[m] - soil

	Wave speed [m/s]	Distance [m]			
		7.78	9.78	23.78	12.67
		Arrival time [s]	Approx. reflection time [s]		
			iFEM	FEM	rock layer
Comp. wave	1690	0.0046	0.0058	0.014	0.0076
Shear wave	228	0.034	0.043	0.10	0.056
Rayleigh wave	211	0.037	0.046	0.11	0.060

Table 5: Distance measure from load corner point $[0.50.50]^T$ m to observation point with corresponding wave arrival times

The calculation is as in the example before performed using the presented infinite element (denoted as "iFEM, all wave types (c_1, c_S, c_R)" in the following plots), with the shape functions given in (20). In figure 12(a) and (b), the vertical solid displacement u_3 is depicted, whereas the horizontal solid displacement u_1 is shown in figure 13. Note that the horizontal displacement u_2 is equal to u_1 due to the symmetry of the considered problem. The correct representation of the wave arrivals of the proposed method was already discussed in the example before and will be not mentioned again. Whereas the expected arrival of reflected compressional waves from the rock layer ($t = 0.0076$ s) is nearly not detectable, the influence of reflected shear waves is clearly observable at time $t = 0.056$ s in figure 12(b). Since the influence of the Rayleigh wave is decreasing with depth the displacement change at time $t = 0.060$ s is essentially caused by the shear wave alone (arrival time $t = 0.056$ s). Since up to this time the influence of the compressional wave is of minor influence the deviation of the pure FEM calculation is relatively small.

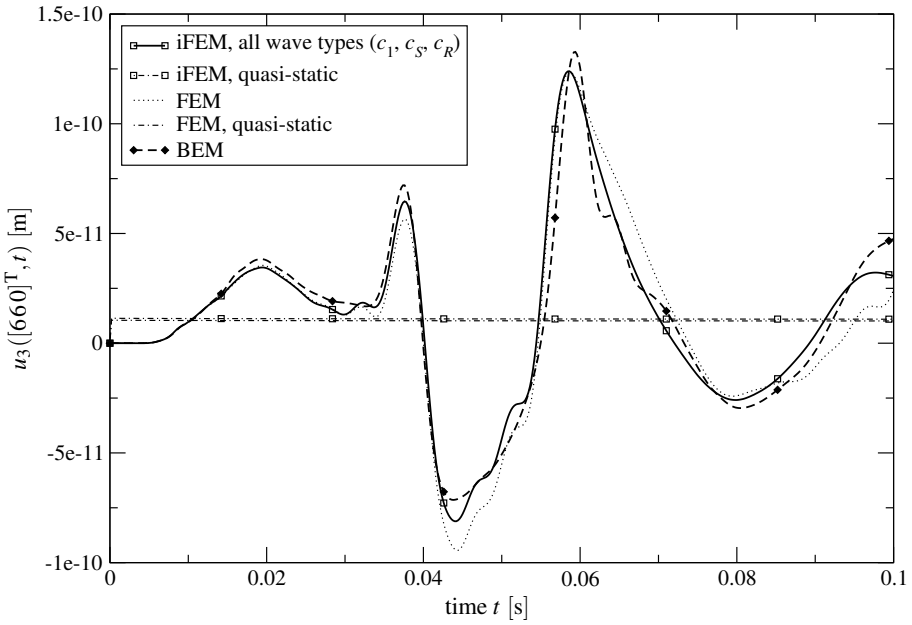

(b) Zoom section of 12(a) - Solid displacement u_3 at observation point $[660]^T$[m] - soil

Figure 12: Vertical solid displacement u_3 at observation point $[660]^T$[m] - soil

This behavior changes as the reflected shear- and Rayleigh wave from the FEM boundary reach the observation point at time $t = 0.10\,\mathrm{s}$ and $t = 0.11\,\mathrm{s}$. From this time on, the pure FEM results diverge from the calculation using infinite elements which can be clearly noticed in figures 12(a) and 13. Also, the behavior of the solution with the infinite elements differs from the BEM solution, which is due to the fact that the infinite elements just try to approximate the far field behavior. Consequently, the far field is represented in another fashion. With ongoing time the solutions approach the quasi-static equilibrium state since the introduced waves are transferred to infinity. This is not the case for the pure FEM solution where still reflected waves can be noticed. Of course, when enough time has passed the damping due to the material will also cause this solution to approach the quasi-static equilibrium. It must be mentioned that the quasi-static solutions of the calculation with the infinite elements and the pure FEM coincidence proper. Only the BEM solution approaches another quasi-static equilibrium.

8 Conclusion

An infinite element has been developed for wave propagation problems in semi-infinite poroelastic media. The saturated porous media is modeled based on Biot's theory. Infinite elements are used to describe the behavior of the far field, whereas the near field is described through conventional finite elements. The infinite elements are constructed in such a way that the Sommerfeld radiation condition is approximated, i.e., the waves decay with distance and are not reflected at infinity. The mapping from the physical space to the local space models a $1/r$-like behavior. The shape functions are formulated in Laplace domain with exponential functions

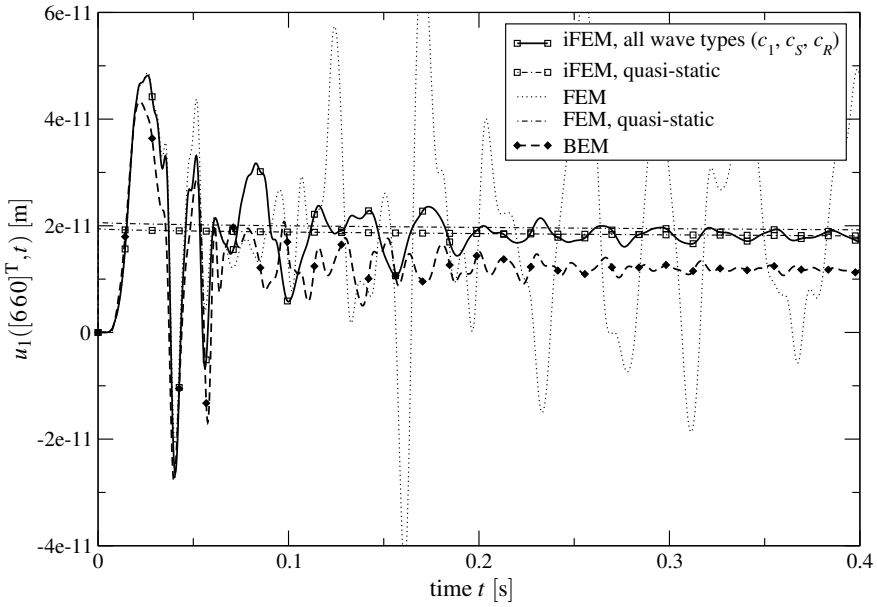

Figure 13: Horizontal solid displacement $u_1 (= u_2)$ at observation point $[660]^{\mathrm{T}}$[m] - soil

for each wave type. To evaluate the occurring integrals, containing these exponential functions, in the variational formulation a special quadrature rule has been derived. To gain a time domain solution of the far field the convolution quadrature method is used for the inverse Laplace transformation. The temporal behavior of the near field is calculated using standard time integration schemes, e.g., the Newmark-method. Finally, the near and far field has been combined using a substructure technique for any time step. The proper functionality of the proposed infinite element is demonstrated for a poroelastic column and a halfspace with different boundary conditions.

Acknowledgement The authors gratefully acknowledges the financial support by the Austrian Science Fund (FWF) under grant P18481-N13.

A One dimensional analytic solution

The derivation of the one-dimensional analytic solution of a poroelastic column follows basically the procedure shown in [45]. Thus, inserting the flux (3b) into (2) yields together with (3a) a set of coupled homogeneous ordinary differential equations

$$\left(K + \tfrac{4}{3}G\right)\hat{u}_{,xx} - \alpha\hat{p}_{,x} - s^2\rho\hat{u} = 0$$
$$-\kappa\left[\hat{p}_{,xx} + \rho_f s^2 \hat{u}_{i,i}\right] + s\alpha\hat{u}_{,x} + s\frac{\phi^2}{R}\hat{p} = 0\,,$$

where also the Laplace transformation is applied and vanishing initial conditions are assumed. Inserting the ansatz

$$\begin{bmatrix} \hat{u}(x,s) \\ \hat{p}(x,s) \end{bmatrix} = \mathrm{e}^{s\lambda x} C\mathbf{v}$$

with the Eigenvector $\mathbf{v}$ into the set of differential equations (27) yields the solution of the form

$$\begin{bmatrix} \hat{u}(x,s) \\ \hat{p}(x,s) \end{bmatrix} = C_1\mathbf{v}^1\,\mathrm{e}^{s\lambda_1 x} + C_2\mathbf{v}^2\,\mathrm{e}^{s\lambda_2 x} + C_3\mathbf{v}^3\,\mathrm{e}^{-s\lambda_1 x} + C_4\mathbf{v}^4\,\mathrm{e}^{-s\lambda_2 x}\,. \tag{28}$$

The Eigenvalues λ_i are the inverse of the compressional wave speeds and are defined in (8), thus $\lambda_i = 1/c_i$ holds. Furthermore, the relation $\lambda_3 = -\lambda_1$ and $\lambda_4 = -\lambda_2$ is used. The corresponding Eigenvectors are defined as

$$\mathbf{v}^i = \begin{bmatrix} 1 \\ \frac{(K+\frac{4}{3}G)s\lambda_i^2 - s\rho}{\alpha\lambda_i} \end{bmatrix} = \begin{bmatrix} v_1^i \\ v_2^i \end{bmatrix}. \tag{29}$$

The constants C_i in (28) may be determined in accordance to the underlying physical problem. Note that the result contains both leftward and rightward traveling waves, or in other words, the solution consists of terms with increasing and decreasing amplitude. This is obvious, since the real part of the Laplace parameter s is by definition always larger than zero, i.e., $\mathrm{Re}(s) > 0$. It can be verified that for the real part of the fraction $s/c_i > 0$ holds. In order to fulfill the radiation condition only the outward traveling waves with decreasing amplitude are allowed [31, 32]. Thus, the solution of an infinite poroelastic column is

$$\begin{bmatrix} \hat{u}(x,s) \\ \hat{p}(x,s) \end{bmatrix} = C_3\mathbf{v}^3\,\mathrm{e}^{-s\lambda_1 x} + C_4\mathbf{v}^4\,\mathrm{e}^{-s\lambda_2 x}\,. \tag{30}$$

B Analytic 1D poroelastodynamic infinite element

The analytic poroelastic infinite element is obtained by a simple Dirichlet to Neumann map. In other words, a relation between the nodal displacements and the nodal stresses as well as for the nodal pressure and the nodal flux is performed. The analytic infinite poroelastic element, as depicted in figure 14, is deduced from the general analytic solution of an infinite porous rod, given by (30). Thus, the general ansatz of the analytic infinite element is

$$\begin{bmatrix} \hat{u}(x,s) \\ \hat{p}(x,s) \end{bmatrix} = C_3 \begin{bmatrix} 1 \\ v_2^3 \end{bmatrix} \mathrm{e}^{-s\lambda_1 x} + C_4 \begin{bmatrix} 1 \\ v_2^4 \end{bmatrix} \mathrm{e}^{-s\lambda_2 x}\,, \tag{31}$$

with the Eigenvectors defined in (29). Inserting the boundary conditions

$$\hat{u}(0,s) = \hat{u}^i \quad , \quad \hat{p}(0,s) = \hat{p}^i$$

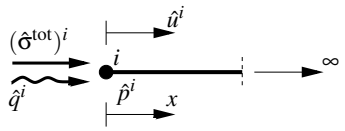

Figure 14: Analytic infinite poroelastic element

into (31) yields the constants

$$C_3 = \frac{v_2^4 u^i - p^i}{v_2^4 - v_2^3} \quad , \quad C_4 = \frac{p^i - v_2^3 u^i}{v_2^4 - v_2^3}$$

and, further on, the solution for the solid displacement and the pore pressure

$$\begin{bmatrix} \hat{u}(x,s) \\ \hat{p}(x,s) \end{bmatrix} = \frac{v_2^4 u^i - p^i}{v_2^4 - v_2^3} \mathbf{v}^3 \, \mathrm{e}^{-s\lambda_1 x} + \frac{p^i - v_2^3 u^i}{v_2^4 - v_2^3} \mathbf{v}^4 \, \mathrm{e}^{-s\lambda_2 x} \ . \tag{32}$$

The corresponding stress is obtained by inserting the solution (32) into the one-dimensional form of the Laplace transformed constitutive relation (1)

$$\begin{aligned} \hat{\sigma}^{\mathrm{tot}}(x,s) &= (K + \tfrac{4}{3}G)\hat{u}_{,x}(x,s) - \alpha \hat{p}(x,s) \\ &= -s(K + \tfrac{4}{3}G) \left[\lambda_1 \frac{v_2^4 u^i - p^i}{v_2^4 - v_2^3} \, \mathrm{e}^{-s\lambda_1 x} + \lambda_2 \frac{p^i - v_2^3 u^i}{v_2^4 - v_2^3} \, \mathrm{e}^{-s\lambda_2 x} \right] - \alpha \hat{p}(x,s) \end{aligned}$$

and the one-dimensional flux is defined by

$$\begin{aligned} \hat{q}(x,s) &= -\kappa \left[\hat{p}_{,x}(x,s) + s^2 \rho_f \hat{u}(x,s) \right] \\ &= -\kappa \left[s\lambda_1 \frac{v_2^4 u^i - p^i}{v_2^4 - v_2^3} v_2^3 \, \mathrm{e}^{-s\lambda_1 x} + s\lambda_2 \frac{p^i - v_2^3 u^i}{v_2^4 - v_2^3} v_2^4 \, \mathrm{e}^{-s\lambda_2 x} + s^2 \rho_f \hat{u}(x,s) \right] . \end{aligned}$$

The next step is to incorporate the nodal total stress $(\hat{\sigma}^{\mathrm{tot}})^i$ and flux q^i, where the superscript denotes the respective node. This is realized by the boundary conditions stated at node i as

$$\hat{\sigma}^{\mathrm{tot}}(0,s) = -(\hat{\sigma}^{\mathrm{tot}})^i \quad , \quad \hat{q}(0,s) = \hat{q}^i \ .$$

Hence, the nodal relation of the single components is given by

$$\begin{bmatrix} (\hat{\sigma}^{\mathrm{tot}})^i \\ \hat{q}^i \end{bmatrix} = \frac{1}{(v_2^3 - v_2^4)} \begin{bmatrix} s(K + \frac{4}{3}G)\left(v_2^3 \lambda_2 - v_2^4 \lambda_1\right) & \alpha(v_2^3 - v_2^4) + (K + \frac{4}{3}G)s(\lambda_1 - \lambda_2) \\ s\kappa\left[s v_2^4 \rho_f - v_2^3\left(v_2^4(\lambda_1 - \lambda_2) - s\rho_f\right)\right] & s\kappa\left(v_2^3 \lambda_1 - v_2^4 \lambda_2\right) \end{bmatrix} \begin{bmatrix} \hat{u}^i \\ \hat{p}^i \end{bmatrix} .$$

The above relation is now appropriate to be attached to an one-dimensional poroelastic finite element formulation of the form presented in section 3 in Laplace domain.

References

[1] D. E. Amos. Algorithms 683: A portable FORTRAN subroutine for exponential integrals of a complex argument. *ACM Transactions on Mathematical Software*, 16(2):178–182, 1990.

[2] D. E. Amos. Computation of exponential integrals of a complex argument. *ACM Transactions on Mathematical Software*, 16(2):169–177, 1990.

[3] H. G. Askar. Infinite elements for ground freezing problems. *Journal of Engineering Mechanics ASCE*, 110(2):157–172, 1984.

[4] R. J. Astley. Infinite elements for wave problems: a review of current formulations and an assessment of accuracy. *International Journal for Numerical Methods in Engineering*, 49: 951–976, 2000.

[5] R. J. Astley, G. J. Macaulay, J.-P. Coyette, and L. Cremers. Three-dimensional wave-envelope elements of variable order for acoustic radiation and scattering. Part I: Formulation in the frequency domain. *Journal of the Acoustical Society of America*, 103(1):49–63, 1998.

[6] I. Babuška. Error-bounds for finite element method. *Numerische Mathematik*, 16(4):322–333, 1971.

[7] I. Babuška. The finite element method with Lagrangian multipliers. *Numerische Mathematik*, 20(3):179–192, 1973.

[8] U. Basu. Explicit finite element perfectly matched layer for transient three-dimensional elastic waves. *International Journal for Numerical Methods in Engineering*, 77(2):151–176, 2009.

[9] U. Basu and A. K. Chopra. Perfectly matched layers for time-harmonic elastodynamics of unbounded domains: theory and finite-element implementation. *Computer Methods in Applied Mechanics and Engineering*, 192:1337–1375, 2003.

[10] U. Basu and A. K. Chopra. Perfectly matched layers for transient elastodynamics of unbounded domains. *International Journal for Numerical Methods in Engineering*, 59:1039–1074, 2004.

[11] T. Belytschko, H. J. Yen, and R. Mullen. Mixed methods for time integration. *Computer Methods in Applied Mechanics and Engineering*, 17(18):259–275, 1979.

[12] T. Belytschko, P. Smolinski, and W. K. Liu. Stability of multi-time step partitioned integrators for first-order finite element systems. *Computer Methods in Applied Mechanics and Engineering*, 49(3):281–297, 1985.

[13] J.-P. Berenger. A perfectly matched layer for the absorption of electromagnetic waves. *Journal of Computational Physics*, 114:185–200, 1994.

[14] P. Bettess and O. C. Zienkiewicz. Diffraction and refraction of surface waves using finite and infinite elements. *International Journal for Numerical Methods in Engineering*, 11(8): 1271–1290, 1977.

[15] M. A. Biot. Theory of Propagation of Elastic Waves in a Fluid-Saturated Porous Solid. II. Higher-Frequency-Range. *Journal of the Acoustical Society of America*, 28(2):179–191, 1956.

[16] M. A. Biot. Theory of Propagation of Elastic Waves in a Fluid-Saturated Porous Solid. I. Low-Frequency-Range. *Journal of the Acoustical Society of America*, 28(2):168–178, 1956.

[17] F. Brezzi. On the existence, uniqueness and approximation of saddle-point problems arising from Lagrangian multipliers. *RAIRO Anal. Numer*, 8(2):129–151, 1974.

[18] J. Chen and G. F. Dargush. Boundary element method for dynamic poroelastic and thermoelastic analyses. *International Journal of Solids and Structures*, 32(15):2257–2278, 1995.

[19] W. C. Chew, J.M. Jin, and E. Michielssen. Complex coordinate stretching as a generalized absorbing boundary condition. *Microwave and Optical Technology Letters*, 15(6):363–369, 1997.

[20] Y. K. Chow and I. M. Smith. Static and periodic infinite solid elements. *International Journal for Numerical Methods in Engineering*, 17:503–526, 1981.

[21] Z. Chuhan and Z. Chongbin. Coupling method of finite and infinite elements for strip foundation wave problems. *Earthquake Engineering and Structural Dynamics*, 15:839–851, 1987.

[22] G. Doetsch. *Anleitung zum praktischen Gebrauch der Laplace-Transformation und der Z-Transformation*. R. Oldenbourg Verlag, München, Wien, 6. Auflage, 1989.

[23] D. Dreyer. *Efficient infinite elements for exterior acoustics*. PhD thesis, Technische Universität Hamburg-Harburg, 2004.

[24] D. Dreyer and O. von Estorff. Improved conditioning of infinite elements for exterior acoustics. *International Journal for Numerical Methods in Engineering*, 58(6):933–953, 2003.

[25] C. Emson and P. Bettess. Application of infinite elements to external electromagnetic field problems. In *Proc. Int. Conf. Num. Meth. Coupled Problems, E. Hinton et al. (eds), Pineridge Press*, pages 887–902, 1981.

[26] D. Givoli. Non-reflecting boundary conditions. *Journal of Computational Physics*, 94: 1–29, 1991.

[27] D. Givoli. Numerical methods for problems in infinite domains. *Studies in Applied Mechanics*, Elsevier, 1992.

[28] K. F. Graff. *Wave Motion in Elastic Solids*. Oxford University Press, 1975.

[29] T. J. R. Hughes. *The Finite Element Method: Linear, Static and Dynamic Finite Element Analysis*. Dover Publications - Mineola, New York, 2000.

[30] M. Jung and U. Langer. *Methode der finiten Elemente für Ingenieure*. 1. Auflage. B. G. Teubner GmbH, Stuttgart/Leipzig/Wiesbaden, 2001.

[31] N. Khalili, S. Valliappan, J. T. Yazdi, and M. Yazdchi. 1D infinite element for dynamic problems in saturated porous media. *Communications in Numerical Methods in Engineering*, 13(9):727–738, 1997.

[32] N. Khalili, M. Yazdchi, and S. Valliappan. Wave propagation analysis of two-phase saturated porous media using coupled finite-infinite element method. *Soil Dynamics and Earthquake Engineering*, 18:533–553, 1999.

[33] Y. K. Kim and H. B. Kingsbury. Dynamic characterization of poroelastic materials. *Experimental Mechanics*, 19(7):252–258, 1979.

[34] R. W. Lewis and B. A. Schrefler. *The Finite Element Method in the Static and Dynamic Deformation and Consolidation of Porous Media*. John Wiley and Sons, Chichester, 1998.

[35] J. Lysmer and R. L. Kuhlemeyer. Finite dynamic model for infinite media. In *Proceedings of the American Society of Civil Engineers (ASCE)*, pages 859–877, 1969.

[36] B. Markert, Y. Heider, and W. Ehlers. Comparison of monolithic and splitting solution schemes for dynamic porous media problems. *International Journal for Numerical Methods in Engineering*, 82(11):1341–1383, 2010.

[37] J. M. M. C. Marques and D. R. J. Owen. Infinite elements in quasi-static materially nonlinear problems. *Computers & Structures*, 18(4):739–751, 1984.

[38] F. Medina and J. Penzien. Infinite elements for elastodynamics. *Earthquake Engineering and Structural Dynamics*, 10:699–709, 1982.

[39] F. Medina and R. L. Taylor. Finite element techniques for problems of unbounded domains. *International Journal for Numerical Methods in Engineering*, 19:1209–1226, 1983.

[40] N. M. Newmark. A method of computation for structural dynamics. *JEMD*, 85:67–93, 1959.

[41] R. Rajapakse and P. Karasudhi. An efficient elastodynamic infinite element. *International Journal of Solids and Structures*, 22(6):643–657, 1986.

[42] J. W. S. Rayleigh. On waves propagated along the plane surface of an elastic solid. *Proceedings of the London mathematical Society*, 17:4–11, 1887.

[43] Z. S. Sacks, D. M. Kingsland, R. Lee, and J. F. Lee. A perfectly matched anisotropic absorber for use as an absorbing boundary condition. *IEEE Antennas and Propagation Society magazine*, 43(12):1460–1463, 1995.

[44] M. Schanz. *Wave Propagation in Viscoelastic and Poroelastic Continua: A Boundary Element Approach*, volume 2 of *Lecture Notes in Applied Mechanics*. Springer-Verlag, Berlin, Heidelberg, New York, 2001.

[45] M. Schanz and A. H.-D. Cheng. Transient wave propagation in a one-dimensional poroelastic column. *Acta Mechanica*, 145(1-4):1–18, 2000.

[46] M. Schanz and D. Pryl. Dynamic fundamental solutions for compressible and incompressible modeled poroelastic continua. *International Journal of Solids and Structures*, 41(15): 4047–4073, 2004.

[47] B. R. Simon, J. S.-S. Wu, O. C. Zienkiewicz, and D. K. Paul. Evaluation of $u-w$ and $u-\pi$ finite element methods for the dynamic response of saturated porous media using one-dimensional models. *International Journal for Numerical and Analytical Methods in Geomechanics*, 10(5):461–482, 1986.

[48] L. Simoni and B. A. Schrefler. Mapped infinite elements in soil consolidation. *International Journal for Numerical Methods in Engineering*, 24:513–527, 1987.

[49] J. M. Sullivan Jr. and K. O'Neill. Application of infinite elements to phase change situations on deforming meshes. *International Journal for Numerical Methods in Engineering*, 33(9):1861–1874, 1992.

[50] R. F. Ungless. An infinite finite element. *MA Sc Thesis, University of British Columbia*, 1973.

[51] O. von Estorff and M. Firuziaan. Nonlinear dynamic response by coupling BEM and FEM. *Engineering Analysis with Boundary Elements*, 24(10):715–725, 2000.

[52] E. W. Weisstein. Exponential Integral. *From MathWorld–A Wolfram Web Resource.* `http://mathworld.wolfram.com/ExponentialIntegral.html` and `http://functions.wolfram.com/GammaBetaErf/ExpIntegralEi`.

[53] Wolfram Research, Inc. *Mathematica, Version 6.0*. Champaign, Illinois, 2007.

[54] J. Yang. A note on Rayleigh wave velocity in saturated soils with compressible constituents. *Canadian Geotechnical Journal*, 38(6):1360–1365, 2001.

[55] Y.-B. Yang, S.-R. Kuo, and H.-H. Hung. Frequency-independent infinite elements for analysing semi-infinite problems. *International Journal for Numerical Methods in Engineering*, 39:3553–3569, 1996.

[56] C.-B. Yun, J.-M. Kim, and C.-H. Hyun. Axisymmetric elastodynamic infinite elements for multi-layered half-space. *International Journal for Numerical Methods in Engineering*, 38 (22):3723–3743, 1995.

[57] Y. Q. Zeng, J. Q. He, and Q. H. Liu. The application of the perfectly matched layer in numerical modeling of wave propagation in poroelastic media. *Geophysics*, 66(4):1258–1266, 2001.

[58] C. Zhao and S. Valliappan. A dynamic infinite element for three-dimensional infinite-domain wave problems. *International Journal for Numerical Methods in Engineering*, 36 (15):2567–2580, 1993.

[59] C. Zhao and S. Valliappan. Transient infinite elements for contaminant transport problems. *International Journal for Numerical Methods in Engineering*, 37(7):1143–1158, 1994.

[60] C.-B. Zhao, C.-H. Zhang, and G.-D. Zhang. Analysis of 3-d foundation wave problems by mapped dynamic infinite elements. *Science in China (Series A)*, 32(4):479–491, 1989.

[61] Y. Zheng and X. Huang. Anisotropic Perfectly Matched Layers for Elastic Waves in Cartesian and Curvilinear Coordinates. Research report, Earth Resource Laboratory, Dept. of Earth, Atmospheric, and Planetary Sciences , Massachusetts Institute of Technology, 2002. URL `http://www-eaps.mit.edu/erl/research/report1/pdf2002/ZHENG.pdf`.

[62] O. C. Zienkiewicz and P. Bettess. *Fluid Structure Interaction*, chapter 5. Numerical methods in offshore engineering. John Wiley, 1978.

[63] O. C. Zienkiewicz and T. Shiomi. Dynamic behaviour of saturated Porous Media; The generalized Biot Formulation and its Numerical Solution. *International Journal for Numerical and Analytical Methods in Geomechanics*, 8:71–96, 1984.

[64] O. C. Zienkiewicz, C. T. Chang, and P. Bettess. Drained, undrained, consolidating and dynamic behavior assumptions in soils. *Geotechnique*, 30:385–395, 1980.

[65] O. C. Zienkiewicz, C. Emson, and P. Bettess. A novel boundary infinite element. *International Journal for Numerical Methods in Engineering*, 19(3):393–404, 1983.

[66] O. C. Zienkiewicz, K. Bando, P. Bettess, C. Emson, and T. C. Chiam. Mapped infinite elements for exterior wave problems. *International Journal for Numerical Methods in Engineering*, 21:1229–1251, 1985.

[67] O. C. Zienkiewicz, A. H. C. Chan, M. Pastor, B. A. Schrefler, and T. Shiomi. *Computational Geomechanics*. John Wiley & Sons, 1999.

[68] O. C. Zienkiewicz, R. L. Taylor, and J. Z. Zhu. *The Finite Element Method: Its Basis and Fundamentals*. Elsevier Butterworth-Heinemann, sixth edition edition, 2005.